European Journal of Agronomy 173 (2026) 127909

Contents lists available at ScienceDirect

European Journal of Agronomy

journal homepage: www.elsevier.com/locate/eja

Future climate change increases the risk of wheat yield loss due to agricultural drought in southeastern Australia

Keyu Xiang [a,b], Bin Wang [b,c,d,*], De Li Liu [b,d,e,*], Chao Chen [f], Fei Ji [g], Shijin Yao [a,b], Siyi Li [h], Alfredo Huete [a], Yi Li [i], Qiang Yu [j,**]

[a] School of Life Sciences, Faculty of Science,, University of Technology Sydney, PO Box 123, Broadway, Sydney, NSW 2007, Australia
[b] NSW Department of Primary Industries, Wagga Wagga Agricultural Institute, Wagga Wagga, NSW 2650, Australia
[c] Hawkesbury Institute for the Environment, Western Sydney University, Richmond, NSW 2753, Australia
[d] Gulbali Institute for Agriculture, Water and Environment, Charles Sturt University, Wagga Wagga, NSW 2650, Australia
[e] Climate Change Research Centre, University of New South Wales, Sydney, NSW 2052, Australia
[f] CSIRO Agriculture and Food, Private Bag 5, PO, Wembley, WA 6913, Australia
[g] Science and Insights Division, NSW Department of Climate Change, Energy, the Environment and Water, Lidcombe, NSW 2141, Australia
[h] School of Agriculture and Food Sciences, The University of Queensland, St Lucia, QLD, Australia
[i] College of Water Resources and Architectural Engineering, Northwest A&F University, Yangling, Shaanxi 712100, China
[j] State Key Laboratory of Soil Erosion and Dryland Farming on the Loess Plateau, Northwest A&F University, Yangling, Shaanxi 712100, China

ARTICLE INFO

Keywords:
Climate change
Wheat yield
Plant available water
Agricultural drought
APSIM

ABSTRACT

Agricultural drought poses a significant threat to food security and human sustainability by reducing crop yields, and it is projected to intensify in the future due to ongoing global warming and increasing rainfall variability. As a key contributor to the worldwide food supply, the New South Wales (NSW) wheat belt in southeastern Australia is highly exposed to drought-related risks due to its prevailing dry climate and reliance on the rain-fed cropping system. Yet the future impacts of agricultural drought on regional wheat yields remain poorly quantified under climate change. This study aims to evaluate the risk of wheat yield losses induced by agricultural drought under different climate scenarios, focusing on its spatial distribution and temporal evolution across the NSW wheat belt. We integrated a process-based crop simulation model with a probabilistic approach to assess wheat yield loss risk under future climate scenarios. Agricultural Production System sIMulator (APSIM) model was forced with climate data from multiple Global Climate Models (GCMs), enabling the simulation of long-term wheat yield and plant available water (PAW). The simulated PAW values were standardized to derive SPAWI (Standardized Plant Available Water Index), which was used to characterize drought conditions. Copula functions were then utilized to construct the joint probability distribution between wheat yield and SPAWI, allowing the calculation of yield loss probabilities and the identification of drought trigger thresholds. There was a rising trend in agricultural drought frequency across the wheat belt, especially under the Hot/Dry scenarios. Regional results showed elevated wheat yield loss probabilities in the future, approaching 10 % in the drier and warmer areas. Moreover, the drought index thresholds for triggering wheat yield loss were higher over dry areas but lower in the wet region. Uncertainty attribution analysis identified GCM selection as the primary source of yield loss probability change in arid regions, while in wet regions, the choice of copula function played a more critical role. Our findings show a rising risk of wheat yield loss in the NSW wheat belt under future climate scenarios and reveal substantial spatiotemporal heterogeneity in yield impacts. The results offer critical geographic insights for supporting localized adaptation strategies and evidence-based agricultural planning under drought conditions in the future.

* Corresponding authors at: NSW Department of Primary Industries, Wagga Wagga Agricultural Institute, Wagga Wagga, NSW 2650, Australia.
** Corresponding author.
E-mail addresses: bin.a.wang@dpi.nsw.gov.au (B. Wang), de.li.liu@dpi.nsw.gov.au (D.L. Liu), yuq@nwafu.edu.cn (Q. Yu).

https://doi.org/10.1016/j.eja.2025.127909
Received 25 August 2025; Received in revised form 6 October 2025; Accepted 3 November 2025
Available online 7 November 2025

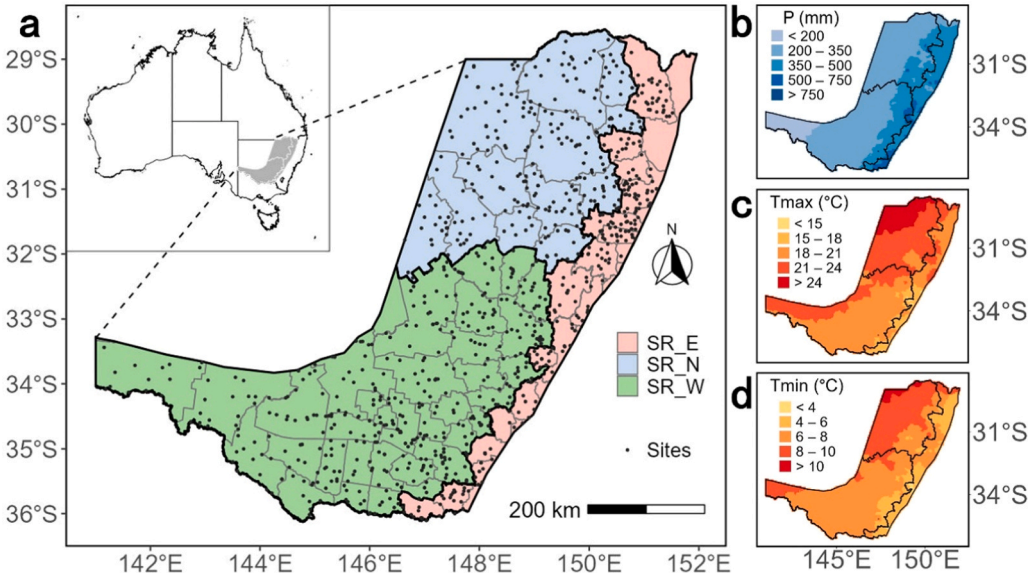

Fig. 1. The spatial distribution of 918 study sites and 3 sub-regions in the NSW wheat belt (a). Historical (1981–2020) mean annual precipitation (P), maximum (Tmax) and minimum temperatures (Tmin) during the wheat growing season (Apr. – Nov.) across the study region (b-d). Grey lines in the map represent the shire boundary of each sub-region.

1. Introduction

Future climate change is projected to result in rising global temperatures and increased precipitation variability (IPCC, 2021; Schaeffer et al., 2025). These changes are expected to intensify both the frequency and severity of drought events (Messori et al., 2025; Wu et al., 2025).

Drought is a multifaceted environmental hazard with complex causal mechanisms and far-reaching consequences, particularly in agricultural systems (Dubey and Ghosh, 2023; Hao et al., 2024; Tang et al., 2024; Wang and Wang, 2023; Zhang et al., 2023b; Zhou et al., 2024). Agricultural drought, defined by insufficient soil moisture for optimal plant growth, poses a serious threat to global food security due to its direct impact on crop yields (Hou et al., 2024; Tefera et al., 2024; Yang et al., 2024), and significantly reduces crop productivity at both global and regional scales (Li et al., 2019; Zhang et al., 2024). For instance, Australia experienced widespread agricultural drought in 2018, resulting in a notable decline in wheat yields due to prolonged soil moisture deficits, particularly across New South Wales (NSW), Australia (Feng et al., 2020b; Xiang et al., 2023). As the frequency and intensity of droughts are projected to escalate under future climate scenarios (Hosseinzadehtalaei et al., 2024; Smith et al., 2024), the stability of agricultural production is expected to face increasing challenges (Wang et al., 2024b). This underscores the need for systematic evaluation of drought impacts on crop productivity within the framework of future climate projections.

The prevailing analytical approaches that assess crop yield response to drought typically incorporate variables such as rainfall, evapotranspiration, and soil moisture to estimate impacts on water availability (Cui et al., 2019; Dietz et al., 2021; Lai et al., 2024; Luo et al., 2023). Compared with other variables such as rainfall reduction or increased evaporative demand due to rising temperatures (Kim et al., 2023; Zhao et al., 2022), soil moisture is a particularly robust factor, as it is closely associated with root-zone conditions and plant physiological processes (Kersebaum and Stöckle, 2022), thus providing more timely warnings of agricultural drought onset (Chen et al., 2020b; Feng et al., 2022; Qing et al., 2022). In addition, the buffer capacity of soil to retain water can mitigate transient rainfall deficits or increased evaporative stress, making it a more reliable predictor of agricultural drought onset and yield impact (Chen et al., 2024; He et al., 2022; Xiang et al., 2025). However, crop yield has been primarily linked to rainfall-based meteorological drought, while soil water-induced agricultural drought has received little attention owing to limited soil moisture data (Gu et al., 2025). Moreover, previous studies have predominantly focused on historical or current yield responses to meteorological drought, with limited evaluation of soil water-induced agricultural drought, especially under different future climate scenarios (Gajurel et al., 2024; Pinke et al., 2022; Rodríguez et al., 2024).

Probabilistic analysis methods have been increasingly applied to assess the impacts of climate change on crop yields, as they can capture dynamic probability changes under various conditions (Li et al., 2025b; Wang et al., 2024b; Xiang et al., 2023). In contrast to deterministic approaches, which typically focus on linear relationships between variables (Geng et al., 2023; Zhao et al., 2024), probabilistic methods rely on joint distribution functions to estimate the likelihood of specific outcomes (Guo et al., 2025b; Seo et al., 2024; Xie et al., 2025). It also facilitates the evaluation of risks associated with extreme events, which are often difficult to capture using deterministic methods (Gao et al., 2025; Han et al., 2024). In addition, probabilistic frameworks allow the estimation of yield loss probabilities and the identification of drought-vulnerable areas based on drought index thresholds, thereby supporting more effective and region-specific responses (Hultgren et al., 2025). Yet, the application of such approaches to agricultural drought in Australia remains scarce, and no study has systematically identified hotspot regions with high yield losses under varying drought intensities.

This study proposes an integrated framework for evaluating the risk of wheat yield reduction resulting from agricultural drought under future climate change by combining a process-based crop model with a joint probability approach. Soil water variation is employed as a primary drought indicator. Using the NSW wheat belt as a case study, we quantitatively examined the spatiotemporal patterns of yield loss probabilities and identified the drought-trigger thresholds under various future climate scenarios. The objectives of this study are threefold: (1) quantifying how the frequency and severity of agricultural droughts have changed over time; (2) assessing how yield loss probabilities and drought thresholds are projected to shift under different climate scenarios; and (3) evaluating the uncertainties associated with these projections. The findings are expected to inform local strategies for mitigating future drought impacts on wheat production and to serve as a reference for agricultural regions with similar climatic conditions facing drought risk.

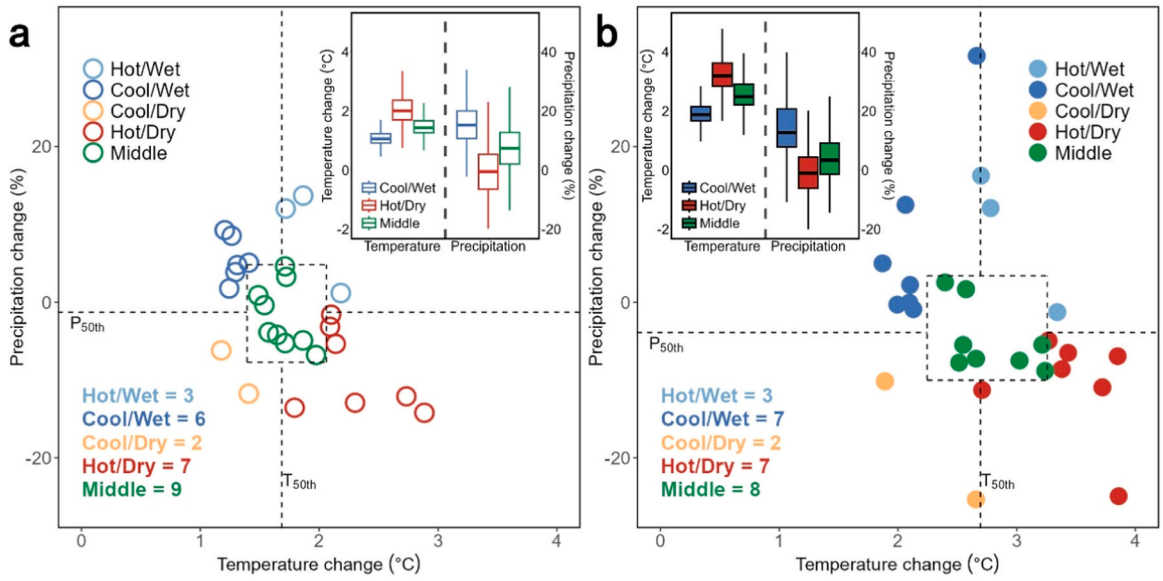

Fig. 2. Change of projected precipitation and mean temperature (2021–2100) in wheat growing season (Apr. – Nov.) relative to the historical period (1981–2020) for 27 GCMs under SSP245 (a) and SSP585 (b) across the NSW wheat belt. Boxplots are the relative change of precipitation and mean temperature for the three selected climate scenarios (i.e., Cool/Wet, Hot/Dry, and Middle) for SSP245 and SSP585. The numbers in (a) and (b) represent the number of GCMs located in each quadrant.

2. Materials and methods

2.1. Study area

The NSW wheat belt is a major grain-producing region in Australia, covering 65 shires and 918 weather sites (Fig. 1a and Table S1), with a cultivated area of approximately 360,000 km^2 (Feng et al., 2018a). The region contributes up to 27 % of the national wheat production (Feng et al., 2018b; Li et al., 2022b; Xiang et al., 2023). Located in south-eastern Australia, the wheat belt is characterized by a Mediterranean climate with notable interannual variability in rainfall and temperature (Fig. 1a) (Wang et al., 2015; Xiang et al., 2025). Geographically, the eastern part of the wheat belt is characterized by mountainous terrain, while the northwest and southwest regions consist primarily of plains. During the historical baseline period (1981–2020), the annual mean values of monthly accumulative rainfall during the wheat growing season (Apr. – Nov.) increased progressively from west to east, ranging from less than 200 mm to over 750 mm, and the annual mean values of monthly average temperature gradually decreased from northwest to southeast, with the highest being above 24℃ and the lowest being below 4℃ (Fig. 1b-d) (http://www.longpaddock.qld.gov.au/silo/ppd/index.php). Based on topographical and meteorological features, we divided the wheat belt into three subregions: the Northern Plains (SR_N), Western Plains (SR_W), and Eastern Slopes (SR_E).

2.2. Climate data

Future climate data were collected from 27 Global Climate Models (GCMs) within the Coupled Model Intercomparison Project version 6 (CMIP6), with specific model details provided in Table S2 (Huang et al., 2022; Shi et al., 2022). Due to the coarse resolution and systematic bias in the original monthly GCM data, a statistical downscaling and bias correction technique proposed by Liu and Zuo (2012) was applied to produce daily-scale meteorological inputs at the site level (Li et al., 2023, 2024). In addition, two Shared Socioeconomic Pathways (SSPs) were employed to represent future climate change scenarios and analyze the projected impacts of agricultural drought on wheat production: SSP2–4.5 (SSP245, an intermediate scenario) and SSP5–8.5 (SSP585, a high-emissions scenario) (Dai et al., 2024; Ruane et al., 2024). SSP245 represents a moderately changing climate, whereas SSP585 reflects more extreme climatic shifts. To assess temporal dynamics, the entire period was divided into three intervals: Baseline (1981–2020), 2040 s (2021–2060), and 2080 s (2061–2100).

Most previous studies assessed climate change impacts based on the median outputs of GCM ensembles, which may overlook substantial variability in climate models (Hultgren et al., 2025; Li et al., 2025a). To better capture the variability across climate projections, we divided the GCMs into five subsets based on the relative change percentiles (25th, 50th, 75th) of annual mean temperature and precipitation during the wheat growing season (Apr. – Nov.): Hot/Wet, Cool/Wet, Cool/Dry, Hot/Dry, and Middle (Bracho-Mujica et al., 2024; Ruane and Mcdermid, 2017). Categorization of the GCM and associated climate characteristics is presented in Fig. 2. We retained all subsets (Hot/Wet, Cool/Wet, Cool/Dry, Hot/Dry, and Middle) for further analysis, 27 GCMs for each SSP. Due to the insufficient sample sizes (the number of GCMs was less than 5) in the Hot/Wet and Cool/Dry subsets, and potential impairments to the robustness of simulation-based yield impact assessments, we therefore presented the results of those two subsets in the supplementary. The main text focuses on the results derived from Cool/Wet, Hot/Dry, and Middle subsets.

2.3. Process-based crop model simulation

Agricultural Production System sIMulator (APSIM) model was employed to simulate soil water and wheat yields (Deihimfard et al., 2023; Holzworth et al., 2014; Jones et al., 2017; Liu et al., 2020). A wheat cultivar of *Sunvale*, a representative cultivar widely adopted in the NSW wheat belt, was selected for growth simulations across all wheat belt sites (Feng et al., 2020a, 2019), and the specific parameters are shown in Table S3. Sowing decisions were guided by an empirical method that reflects regional agronomic practices (Li et al., 2024; Xiang et al., 2025; Zheng et al., 2015), accounting for both sowing window and plan available water (Eqs. S1-2, see supplementary). To mitigate the impacts of extreme soil conditions, a soil type with moderate plant available water capacity (PAWC) was selected from the APSoil database for each site (Table S1) (Dalgliesh et al., 2016; Liu et al., 2014). A uniform sowing density of 120 plants m^{-2} at a depth of 30 mm was applied across all sites (Xiang et al., 2025). Initial nitrate-N and ammonium-N levels were set at 35 kg ha^{-1} and 15 kg ha^{-1}, respectively, with an additional 60 kg ha^{-1} nitrogen fertilizer applied at sowing (Wang et al.,

Table 1
Severity categories of SPAWI.

Drought severity categories	Value range of SPAWI
Normal	(−0.5, 0]
Mild drought	(−1, −0.5]
Moderate drought	(−1.5, −1]
Severe drought	(−2, −1.5]
Extreme drought	(-∞, −2]

2017). Due to the lack of simulation modules for CO_2 concentration in APSIM (Huang et al., 2022), we integrated empirical functions to simulate CO_2 content under different emission scenarios (Eq. S3-4) (Huang et al., 2022; Wang et al., 2024b). Simulations were reinitialized annually to eliminate the "carry-over" effect from the previous season, which can cause the residential influences on soil profiles and affect crop growth (Wang et al., 2017; Xiang et al., 2025), avoiding the sequential change of parameters and ensuring the yield predictions are mainly affected by climate change. The simulated outputs, including wheat yield, growth stage, and plant available water (PAW), were subsequently used for further analysis.

In addition, we collected the observed trial data from the Grains Research and Development Corporation National Variety Trials (GRDC-NVT) to validate the simulation results (Feng et al., 2020a, 2019) (https://nvt.grdc.com.au/), and the detailed information of the collected sites is shown in Table S4. The observed and simulated results during the Baseline period were compared with the coefficient of determination (R^2) and the root mean square error (RMSE) (Fig. S2) (Xiang et al., 2022; Yao et al., 2025).

2.4. Standardized drought index

The standardized drought index has been extensively adopted in drought research as a reliable indicator for monitoring drought conditions (Aghakouchak and Hao, 2014; Bazrafshan et al., 2022; Guo et al., 2025a; Rashid and Beecham, 2019; Vicente-Serrano et al., 2010). It is calculated by fitting the distribution of drought-relevant climatic variables over time and transforming their cumulative distribution values using an inverse standard normal function (Eqs. 1–2) (Farahmand and Aghakouchak, 2015; Yang et al., 2023; Yerdelen et al., 2021), with negative values indicating dryness and positive values denoting wetness. In this study, we applied the standardized index methodology with simulated PAW to develop the Standardized Plant Available Water Index (SPAWI) by using the empirical Gringorten plotting position function to calculate the distribution of the original PAW (Gringorten, 1963), capturing agricultural drought variability in the wheat belt, and the drought index ranges are shown in Table 1. In addition, we employed a back cast method, the past 30 days (approximated 1 month, the minimum length of the calculation process) preceding the end date of the critical wheat growth stage based on the simulation results from APSIM, to calculate SPAWI, thereby addressing the mismatch between calendar months and crop growth stages (Xiang et al., 2025). Consequently, the value of SPAWI for a specific growth stage and scale of each year can be linked to the corresponding annual yield. Specifically, we calculated a 6-month scale SPAWI at the grain filling stage to evaluate the impacts of future climate-induced drought on wheat yield.

$$\mathrm{SAPWI} = \varphi^{-1}(\mathrm{p(x)}) \tag{1}$$

$$\mathrm{p_{PAW}(x_i)} = \frac{\#(\mathrm{x_j} \leq \mathrm{x_i}) - 0.44}{\mathrm{n} + 0.12} \tag{2}$$

where φ^{-1} is the inversed standard normal distribution function; x is the time series of PAW; p is the corresponding empirical probability of x_i; n is the time series length of PAW; i and j are the serial number of n, $1 \leq j \leq n$, and $i = 1, \ldots, n$; # represents the rank of x in decreasing trend. p_{PAW} is probability function of PAW series.

Table 2
Details of selected copula functions.

Copula	Expression	Parameter range
Gaussian	$\Phi_\Sigma[\Phi^{-1}(u), \Phi^{-1}(v)]$	/
t	$t_{\Sigma,\nu}[t_\nu^{-1}(u), t_\nu^{-1}(v)]$	/
Clayton	$(u^{-\theta} + v^{-\theta} - 1)^{-1/\theta}$	$\theta \in [-1, +\infty] \backslash \{0\}$
Gumbel	$\exp\{-[(-\ln u)^\theta + (-\ln v)^\theta]^{1/\theta}\}$	$\theta \geq 1$
Frank	$\frac{1}{\theta}\ln[1 + \frac{(e^{-\theta u} - 1)(e^{-\theta v} - 1)}{e^{-\theta} - 1}]$	$\theta \in R \backslash \{0\}$

2.5. Yield loss probability assessment

Copula functions provide a flexible framework for modelling the joint distribution of several variables by connecting the marginal distributions (Hosseinzadehtalaei et al., 2024; Kanthavel et al., 2022; Sklar, 1973; Tepegjozova et al., 2022). In this study, we utilized wheat yield and SPAWI time series as two distinct variables to fit their respective marginal distributions, and detailed information on the selected candidate marginal distribution functions is summarized in Table S5. And these two distributions were then used to develop a bivariate copula-based joint probability model by fitting the optimal copula functions (Eq. 3) (Li et al., 2022a; Liu et al., 2022). In addition, we adopted several representative copulas that reflect diverse tail-dependence properties for seeking higher accuracy in characterising yield changes under drought extremes (Dißmann et al., 2013; Godfrey et al., 2021; Guo et al., 2025b), and the copula functions used in this study are shown in Table 2. Moreover, the criterion for selecting the optimal copula of yield-index combination is based on the lowest values of the Akaike Information Criterion (AIC) (Sakamoto et al., 1986).

The model was then combined with the conditional probability method to estimate the loss probability of wheat yield under various drought conditions (Eq. 4) (e.g., SPAWI < −0.5, −1, −1.5, −2, −2.5) (Gao et al., 2025; Guo et al., 2025b), the conditional value of yield loss is 20th percentile of the Baseline(1981–2020) wheat yield at shire level. Additionally, by inverting the conditional probability equation (Eq. 4) (Gao et al., 2025; Han et al., 2023), we further estimated the drought trigger thresholds (DT) of SPAWI associated wheat yield loss, based on fixed wheat yield loss levels (Y_c = 20th percentile of the Baseline period) and the defined conditional probability (P_c = 50 %) (Eq. 5). Consequently, the evaluated DT represents the value of SPAWI that causes the wheat yield lower than 20th percentile with 50 % probability. The integrated analysis of loss probabilities and DT provides a comprehensive risk assessment of the impact of agricultural drought on wheat yield in the NSW wheat belt.

$$F_{x,y}(x,y) = C[F_x(x), F_y(y)] \tag{3}$$

$$\mathrm{P(y \leq Y \mid x \leq X)} = \frac{\mathrm{P(y \leq Y,\ x \leq X)}}{\mathrm{P(x \leq X)}} = \frac{\mathrm{C[Fy(Y),\ Fx(X)]}}{\mathrm{Fx(X)}} \tag{4}$$

$$\mathrm{P_c} = \mathrm{P(y \leq Y_c \mid x \leq DT)} = \frac{\mathrm{P(y \leq Y_c,\ X_1 \leq x \leq X_2)}}{\mathrm{P(X_1 \leq x \leq X_2)}} = \frac{\mathrm{C[Fy(Y_c),\ Fx(X_2)]} - \mathrm{C[Fy(Y_c),\ Fx(X_1)]}}{\mathrm{Fx(X_2)} - \mathrm{Fx(X_1)}} \tag{5}$$

where x and y are the SPAWI and wheat yield, respectively; $F(*)$ and $C(*)$ are the marginal distribution function and copula function, respectively; X and Y are conditional values of SPAWI and wheat yield, respectively; P_c is the fixed conditional probability; Y_c is the fixed conditional wheat yield; DT is the drought trigger threshold; X_1 and X_2 are the left and right-side value of SPAWI step interval.

Copula-based joint modelling demands rigorous verification of time series properties to ensure statistical validity and model accuracy (Xiang et al., 2025). Accordingly, we completed a series of diagnostic tests during the model-building process, including correlation analysis between variables (Genest and Favre, 2007), assessment of time series

autocorrelation (Ljung and Box, 1978), distribution fitting tests (Gunar and Trenkler, 1995), and copula goodness-of-fit evaluations (Huang and Prokhorov, 2014; White, 1982). Finally, we used the data that passed all tests for further analysis, and the test results were summarized in Fig. S3.

2.6. Uncertainty analysis

In this study, analysis of variance (ANOVA) was conducted to quantify uncertainties arising from climate models, climate scenarios and the selection of copula function (Li et al., 2025a; Wang et al., 2024a). The key sources of uncertainty included 27 GCMs, 4 climate scenarios (SSP245 and SSP585 for 2040 s and 2080 s, respectively), and 5 copula functions. The independent and interactive effects of these factors on the risk assessment were calculated using Eq. 6.

$$SST = SS_{GCM} + SS_{Scen} + SS_{copula} + SSI_{GCM\times Scen} + SSI_{GCM\times copula} + SSI_{Scen\times copula} + SSI_{GCM\times Scen\times copula} \quad (6)$$

where SST is the total sum of squares of all factors; SS_{GCM}, SS_{Scen}, and SS_{copula} are the separate contributions of GCMs, climate scenarios, and copula functions, respectively; $SSI_{GCM\times Scen}$, $SSI_{Scen\times copula}$, $SSI_{GCM\times copula}$, and $SSI_{GCM\times Scen\times copula}$ are the interaction effects contributed by GCMs, climate scenarios, and copula functions, respectively.

The results obtained at all meteorological sites were spatially extended across the entire wheat belt using the Kriging interpolation method (Workneh et al., 2024). It is important to note that this spatial interpolation was conducted solely to enhance the visual presentation of the results, and no modifications were made to the original data. A schematic overview of the methodological framework in this study is provided in Fig. 3.

3. Results

3.1. Projected change in wheat yields and drought characteristics

The simulated wheat yields under various future climate scenarios (Cool/Wet, Hot/Dry, and Middle subsets) are illustrated in Fig. 4, and the results of Hot/Wet and Cool/Dry subsets are presented in the supplementary materials, the same applies below. Fig. 4a shows wheat yield change (the difference between 2040 s, 2080 s and Baseline, ΔYield) for SR_N, SR_W, and SR_E across the 2040 s and 2080 s, and each box includes all simulation results within each GCM subset and SSP scenario. Under SSP245, yield declines were more pronounced than under SSP585 in the Hot/Dry subset, particularly by the 2040 s. For instance, ΔYield (median value of all sites, as below) during the 2040 s was approximately −150 kg ha^{-1} under SSP585 in SR_N, while under SSP245 in the 2040 s and 2080 s, it ranged from −200 to −210 kg ha^{-1}, respectively. Similar patterns were also observed in SR_W and SR_E. Regionally, ΔYield were highest in SR_N, followed by SR_W, and lowest in SR_E, with interregional differences of up to about 400 kg ha^{-1}. Fig. 4b shows the spatial distribution of ΔYield. Substantial decreases were observed in SR_W, whereas SR_N exhibited relatively extended gains, and large areas experienced yield reductions in the Hot/Dry subset. ΔYield in the Cool/Wet climate subset were notably higher than those in Hot/Dry or Middle subsets, with differences of approximately 300 kg ha^{-1}, respectively. Additionally, the ΔYield under the SSP245 scenario was lower than the simulation results under the SSP585 scenario. In general, the trend of future wheat yield was decreasing under hot and dry conditions, but it showed variations in different regions, scenarios, and GCM subsets.

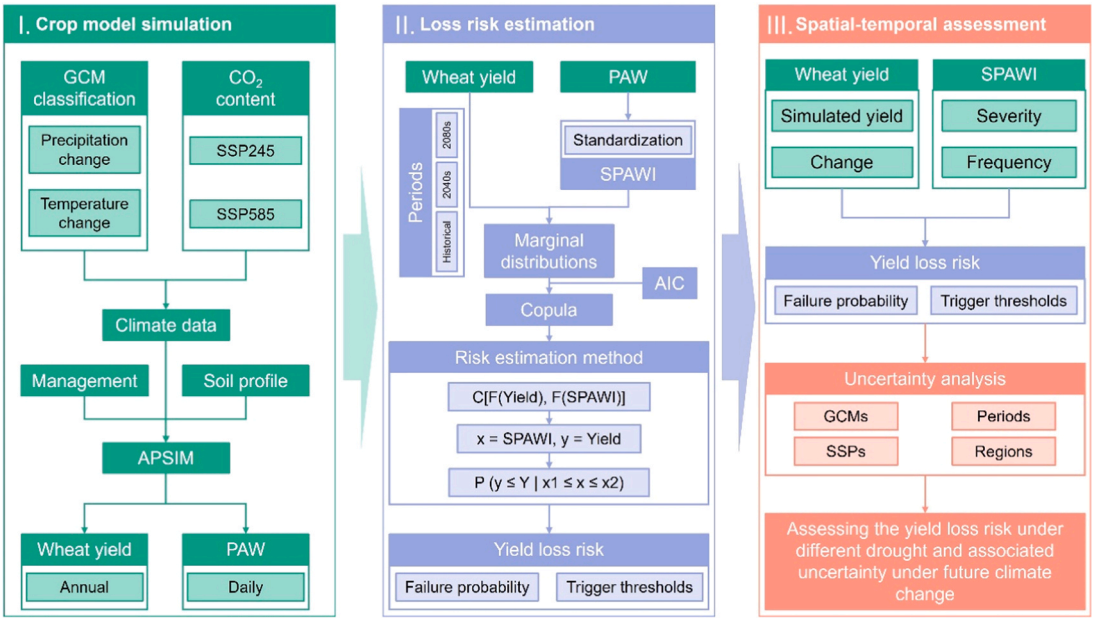

Fig. 3. Flowchart of wheat yield loss probability assessment and uncertainty analysis. GCM, global climate model; APSIM, Agricultural Production System sIMulator; PAW, plant available water; SPAWI, Standardized Plant Available Water Index; AIC, Akaike Information Criterion; F(*), marginal cumulative distribution function; C(*), copula function.

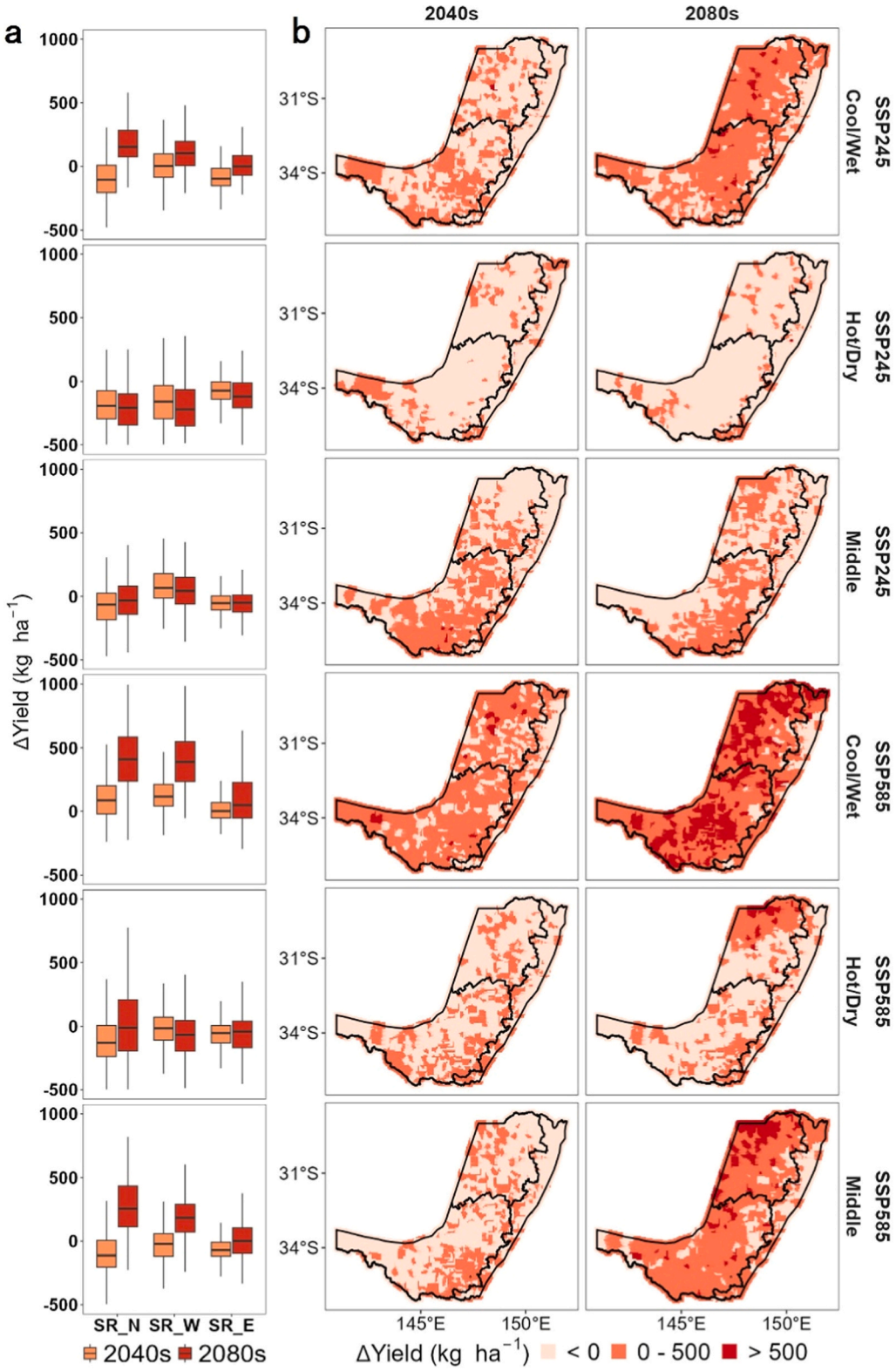

Fig. 4. Simulated wheat yield change (ΔYield) of the 2040 s and 2080 s periods under the SSP245 and SSP585 for Cool/Wet, Hot/Dry, and Middle in three sub-regions (SR_N, SR_W, SR_E) (a). Projected wheat yield change in the 2040 s and 2080 s periods under the SSP245 and SSP585 for Cool/Wet, Hot/Dry, and Middle in the study area (b). The black lines within the box are the median values of simulated yield. The upper and lower boundaries of boxes are the 75th and 25th percentiles, respectively, and the whiskers above or below the box represent the 90th and 10th percentiles.

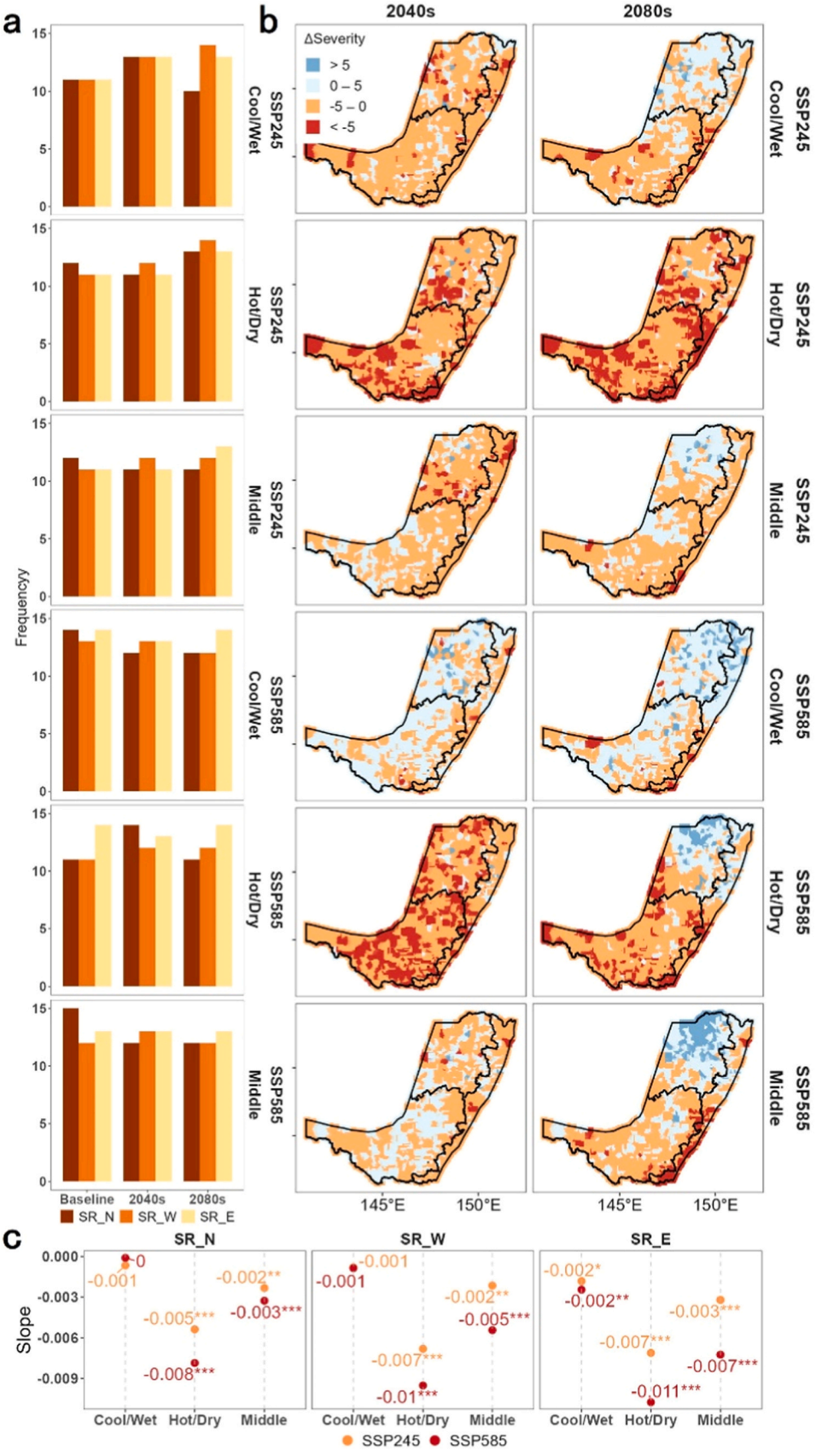

Fig. 5. Projected drought frequency under moderate drought conditions (SPAWI < −1) under different scenarios and three subregions (SR_N, SR_W, SR_E) (a). Projected agricultural drought severity change (ΔSeverity) under moderate drought conditions (SPAWI < −1) in the Baseline, 2040 s and 2080 s periods under the SSP245 and SSP585 for Cool/Wet, Hot/Dry, and Middle in the study area (b). Trend slope of temporal SPAWI from 1981 to 2100 under the SSP245 and SSP585 for Cool/Wet, Hot/Dry, and Middle (c). '*', '**'and '***' indicate the significant level of $p < 0.05$, $p < 0.01$, and $p < 0.001$ for the slopes, respectively.

We derived the Standardized Plant Available Water Index (SPAWI) of the wheat grain filling stage using plant available water (PAW) simulated by APSIM, and its spatiotemporal variability is shown in Fig. 5. Fig. 5a depicts the average drought frequency for each scenario and period (Baseline, 2040 s, 2080 s), with notable differences among GCM subsets. Frequency represents the number of times (years) moderate drought occurs (SPAWI < -1) during each period (40 years). For example, in the Dry/Hot subset, drought occurrences in SR_E were projected to increase from an average of 11–13 times under SSP245 and slightly increased in the Middle subset under SSP585. Drought frequency in SR_N exhibited a downward trend, particularly in the Cool/Wet and Middle subsets, whereas SR_W exhibited slight frequency changes in the Cool/Wet and Middle subsets.

Fig. 5b presents the spatial patterns of accumulated severity change (the difference between 2040 s, 2080 s and Baseline, ΔSeverity) for moderate drought occurrence (SPAWI < -1) across different GCM subsets during each period. Future projections showed an intensification in drought severity in the Hot/Dry subset under both SSP245 and SSP585, with the ΔSeverity of large areas lower than −5. However, drought severity in SR_N was projected to decline progressively, particularly evident in the Cool/Wet and Middle subsets, whereas the southeastern area in SR_E experienced increasing severity across all scenarios. Fig. 5c presents linear trends of SPAWI time series across the entire simulated period (1981–2100), and the slopes were calculated with the median SPAWI values of each GCM subset. In all future scenarios, the simulated SPAWI results showed a decreasing trend, but the magnitude of the decrease varied across different regions and GCM subsets. For instance, SPAWI in the Hot/Dry subset exhibited the steepest negative slopes, approximately −0.01. In contrast, in the Cool/Wet subset, it maintained the less negative slopes around 0, particularly in SR_N and SR_W. Additionally, under SSP585, slopes for all subsets were more negative compared to SSP245. Overall, SPAWI showed a decreasing trend in the future, but there were regional and GCM subset variabilities. Regions more prone to drought were primarily concentrated in the SR_E and SR_W of the wheat belt.

3.2. Risk analysis of wheat yield loss and drought thresholds under climate change

A two-dimensional joint probability distribution was constructed utilizing the paired time series of wheat yield and SPAWI. Conditional probabilities change (the difference between 2040 s, 2080 s and Baseline, ΔProbability) of wheat yield losses under varying drought conditions were then derived from this distribution, as shown in Fig. 6. The map plots illustrate the spatial distribution of ΔProbability under moderate drought conditions (SPAWI < -1), revealing variations among SSP scenarios and GCM subsets. In the Hot/Dry subset, ΔProbability predominantly ranged from 0 % to 50 % under the SSP245 scenario but were generally around −50 % to 0 under SSP585, especially in the 2040 s. In contrast, the Cool/Wet subset showed widespread areas in SR_N and SR_W with the ΔProbability lower than 0. The Middle subset exhibited intermediate characteristics between the Hot/Dry and Cool/Wet subsets, most clearly differentiated in the central areas of the wheat belt. Temporally, the SSP585 scenario indicated a declining trend in yield loss probabilities across all subsets in most areas, whereas the SSP245 scenario exhibited less distinct declines, especially within the Hot/Dry subset.

The corresponding line plots show ΔProbability under different drought conditions (SPAWI $< -0.5, -1, -1.5, -2, -2.5$). The ΔProbability tend to 0 when the drought becomes more severe in all scenarios, as the probability of yield loss will reach 100 % under the extreme drought conditions (SPAWI < -2.5). The ΔProbability were higher under the SSP245 scenarios than under the SSP585 scenarios. Moreover, ΔProbability intensified with the reduction in drought severity, notably in SR_N and SR_W. Overall, the probability of wheat yield loss due to agricultural drought under climate change is projected to decrease in the far future, especially under the SSP585 scenario, but spatial variations exist across regions.

By fixing the yield loss condition (below the 20th percentile at shire level) and applying the conditional probability of 50 % within a SPAWI range of 0 to −3, we estimated the drought threshold (DT) required to trigger wheat yield losses across the entire wheat belt and the difference between 2040 s, 2080 s and Baseline (ΔDT), as depicted in Fig. 7.

Fig. 7a presents spatial distributions of ΔDT. Under the SSP245 scenario, the ΔDT exhibited a similar pattern in the 2040 s and 2080 s, with a range from 0 to 0.5 in most areas of the wheat belt, especially in the Hot-Dry subset. In contrast, most ΔDT were negative under the SSP585 scenario, with the particularly pronounced decreases below −0.5 across the central and northern areas in the Cool/Wet subset. Fig. 7b illustrates the percentage of sites within specific DT ranges relative to the total number of sites in each subregion. The proportion of DT ranging from −2 to −1 is relatively consistent across all scenarios. In contrast, major regional discrepancies were observed primarily within DT ranges of 0 to −1 and −2 to −3. Specifically, SR_N and SR_W had the smallest proportion in the −2 to −3 DT range and the largest in the 0 to −1 range, while SR_E demonstrated the opposite pattern. Additionally, the Cool/Wet subset consistently demonstrated the highest proportion with DT in the −2 to −3 range, followed by the Middle and Hot/Dry subsets. Conversely, the proportion of DT within the 0 to −1 range was highest in the Hot/Dry subset, followed sequentially by the Middle and Cool/Wet subsets. Overall, DT increasingly shifted toward the lower value range (-2 to −3) in future, especially pronounced in the SSP585 scenario.

3.3. Uncertainty analysis of wheat yield loss probability and drought trigger threshold in the future

We further assessed the contribution of uncertainty (%) associated with the selection of GCMs, climate scenarios, and copula functions to the projected wheat yield loss probabilities and DT (Fig. 8). In SR_N, uncertainty due to GCM selection contributed most substantially to the variability in both loss probability (41.9 %) and DT (41.8 %). And the importance of GCM selection declined spatially from SR_W to SR_E, with its effect on loss probability decreasing from 36.5 % (SR_W) to 17.2 % (SR_E). A similar spatial trend was observed for DT, with the GCM influence becoming smaller in SR_E. Conversely, the uncertainty arising from copula function selection exhibited an opposite spatial trend. Specifically, for DT projections, its contribution increased from lower than 5 % in SR_N to 29.2 % in SR_W, and further to 77.1 % in SR_E. Similar spatial patterns of uncertainty occurred for loss probability, with copula-related uncertainties being generally higher in the SR_E (48.4 %). Nevertheless, interaction uncertainties, such as GCM×Scen and Scen×copula, are typically no more than 20 %, while the triple interaction (GCM×Scen×copula) decreases from 22 % (SR_N) to 7.2 % (SR_E) for DT and increases from 6.8 % (SR_N) to 13.1 % (SR_E) for loss probability. Overall, GCM and copula function choices, including their interactions, constituted the major sources of uncertainty, exhibiting distinct regional variations.

4. Discussion

Agricultural drought remains one of the primary contributors to crop yield loss in drought-prone regions (Geng et al., 2023; Slater et al., 2022), and its severity is projected to intensify under future warming scenarios (Gebrechorkos et al., 2025). A better understanding of its projected impacts on wheat yields under climate change is crucial for improving the capacity to manage future food security risks. In this study, we employed a combined approach using process-based crop modelling and conditional probability analysis to assess drought-induced yield loss probability under various climate scenarios in the NSW wheat belt, Australia. Uncertainty sources contributing to the projected results were also assessed. Our results indicate that most

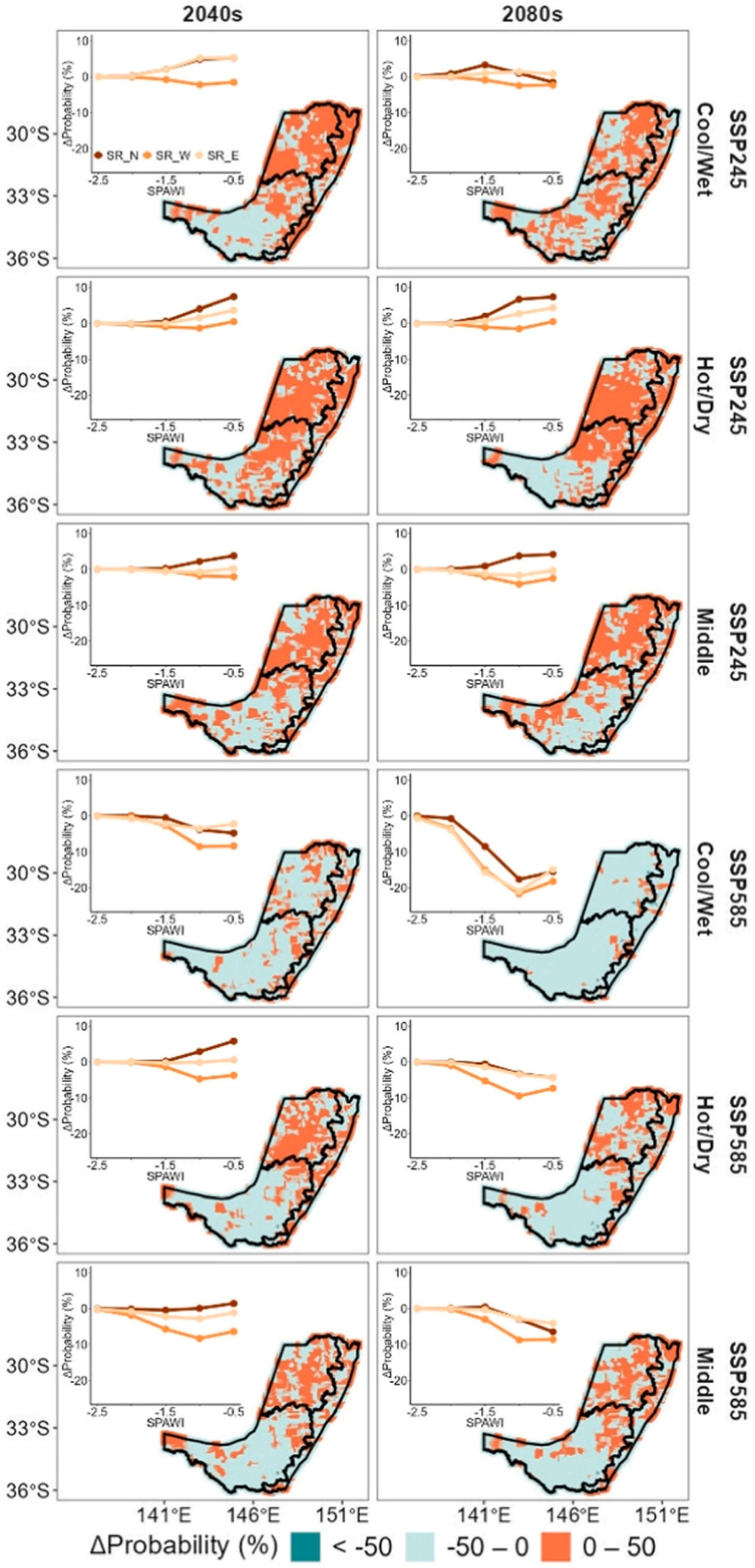

Fig. 6. Projected conditional probability change (ΔProbability) of yield loss under moderate drought conditions (SPAWI < −1) in the Baseline, 2040 s and 2080 s periods under the SSP245 and SSP585 for Cool/Wet, Hot/Dry, and Middle in the study area. Line plots in each plot present the subregional trend for ΔProbability of yield loss under different drought conditions (SPAWI < −0.5, −1, −1.5, −2, −2.5) of corresponding scenarios.

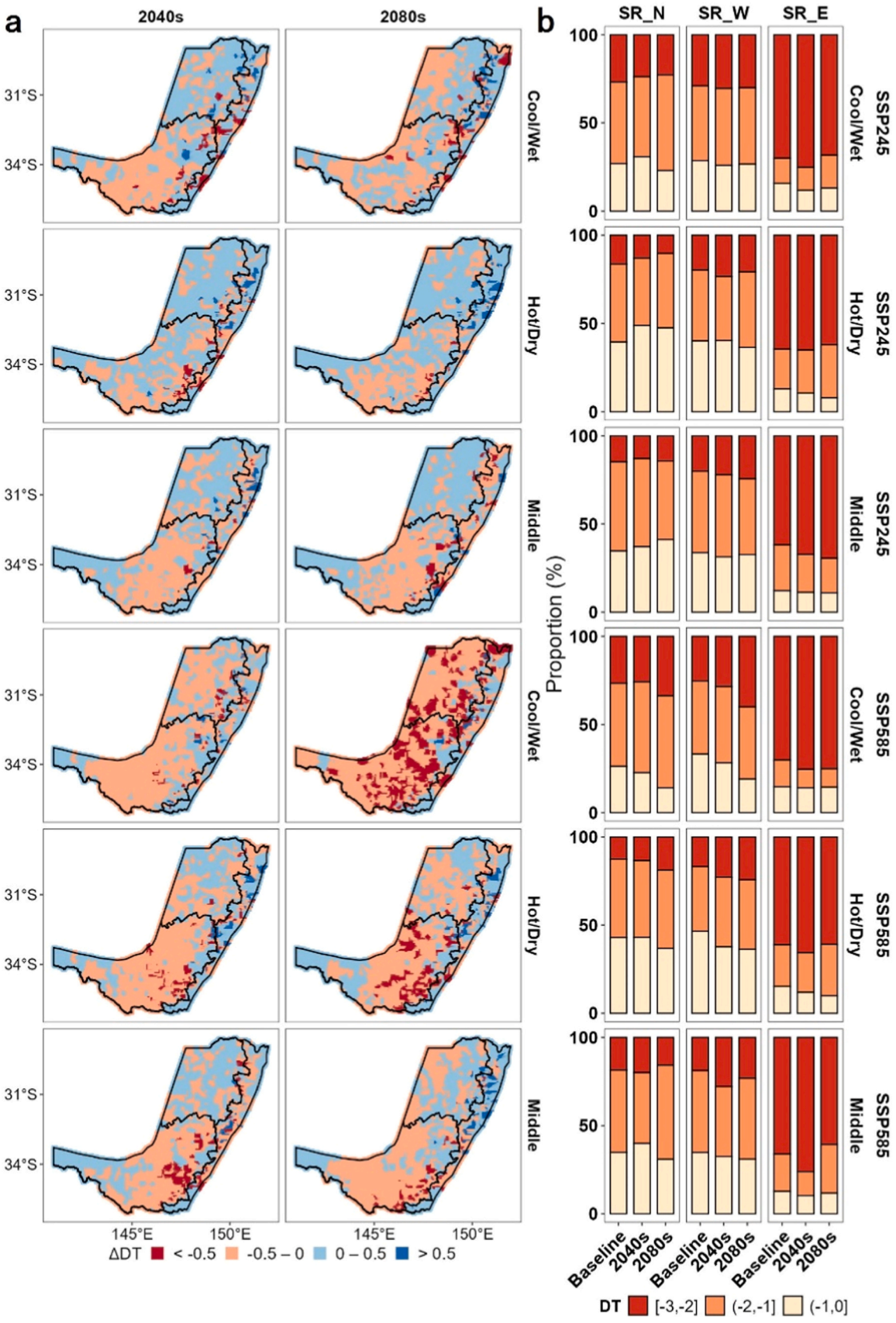

Fig. 7. Projected drought thresholds change (ΔDT) in the Baseline, 2040 s and 2080 s periods under SSP245 and SSP585 scenarios for Cool/Wet, Hot/Dry, and Middle in the study area (a). Proportion of DT in [-3,−2], [[-2,−1] [-[-1, 0]n the Baseline, 2040 s and 2080 s periods under SSP245 and SSP585 scenarios for Cool/Wet, Hot/Dry, and Middle (b).

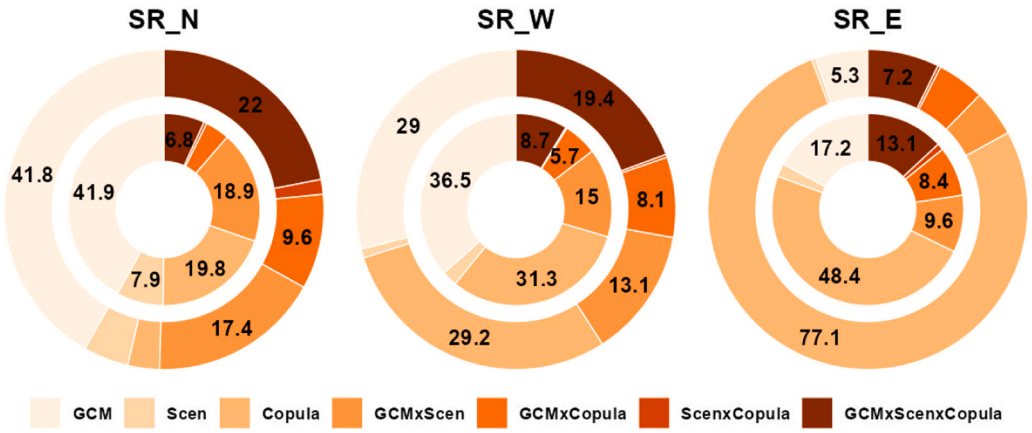

Fig. 8. Sources of uncertainty (%) to the wheat yield loss probability (inner circle) and DT (outer circle) at each subregion. Sources include 27 GCMs, 4 climate scenarios (2 SSPs and 2 future periods), and 5 Copula functions. All specific numbers are displayed in the figure, except for the values that are lower than 5 %. All uncertainty values are statistically significant ($p < 0.001$).

regions within the wheat belt are likely to experience heightened yield loss risks, but the magnitude and distribution of these risks differ between regions, consistent with previous studies (Hou et al., 2024; Yang et al., 2024).

The projected wheat yields under future climate scenarios show an increasing trend across the NSW wheat belt (Fig. 4), with the magnitude of increase varying by region and GCM subsets. Warming accelerates wheat development and leads to a reduction in the length of the individual growth stage (Li et al., 2024), and increased CO_2 concentration improves photosynthetic activity and water-use efficiency, contributing to higher yields (Fan et al., 2023). Notably, the greatest yield gains were achieved under the Cool/Wet subset scenario due to moderate warming and increased rainfall in the SR_N region. It is noteworthy that yield enhancement was also observed in the Hot/Wet subset (Fig. S4), indicating that moisture-enriched environments resulting from higher rainfall levels may facilitate crop productivity in these areas (Zhang et al., 2020). Conversely, in the Hot/Dry or Cool/Dry subset, reduced rainfall negatively affected crop growth, leading to yield losses (Cao et al., 2024; Orlov et al., 2024); however, the CO_2 fertilization effect partially offset these adverse impacts (Fan et al., 2023).

These contrasting outcomes highlight the importance of climatic heterogeneity (Li and Lei, 2022; Malik et al., 2022). Limited water availability combined with high temperature under hot and dry conditions impairs plant physiological processes through stomatal closure, including transpiration and photosynthesis, resulting in reduced yields (Dietz et al., 2021). Under the SSP585 scenario, the CO_2 fertilization effect becomes more impactful (Tausz-Posch et al., 2020; Toreti et al., 2020), particularly under the Cool/Wet subset. However, the mitigation effect observed in the Hot/Wet subset is comparatively weaker than that in the Cool/Wet subset, as most central regions still exhibited yield reductions. Excessive warming may have inhibited crop physiological performance and partially compromised the efficacy of CO_2 fertilization (Mcgrath and Lobell, 2013; Orlov et al., 2024). Moreover, the SPAWI time series reveals an intensifying trend in agricultural drought (Fig. 5 and Fig. S5), consistent with projections for southeastern Australia under future warming (Qiao et al., 2023), such as projected stronger and more persistent droughts (Ukkola et al., 2020).

Our probability-based assessment indicates that as SPAWI values decrease, wheat yield loss probability increases (Fig. 6). The decrease in SPAWI is caused by the decline of plant available water (PAW) and indicates the intensification of drought severity, adversely affecting crop development and biomass accumulation, ultimately reducing yield (He and Wang, 2019; Xiang et al., 2025). However, the pattern of increasing probability exhibits clear spatial variation across the wheat belt. For instance, ΔProbability of SR_N are higher than in SR_W and SR_E, especially in the Hot/Dry under SSP245 and Cool/Dry under SSP585 (Fig. S6). The heightened evapotranspiration demand driven by warming temperatures, coupled with relatively stable precipitation, is increasing greater water stress and higher loss probabilities of wheat yield (Nguyen and Choi, 2023; Zhang et al., 2023a). Although elevated temperatures may shorten wheat growth duration and offer limited avoidance of climate extremes, such as drought (Sun et al., 2024; Ye et al., 2020), the increasing frequency and severity of drought events are expected to weaken the resilience (Ahuja et al., 2022; Dubey and Ghosh, 2023), thereby reducing the effectiveness of such adaptive responses (Tefera et al., 2024). Notably, under the SSP585 scenario in the 2080 s, the loss probability slightly declines, suggesting non-linear temporal dynamics of drought-induced yield loss. Some previous studies attribute this to increasing precipitation that offsets high-temperature stress (Yang et al., 2024). However, our Hot/Dry and Cool/Dry subsets results show stable rainfall levels, implying that the decline in risk may stem from elevated CO_2 concentrations enhancing photosynthetic efficiency in the model (Wei et al., 2023).

Additionally, spatial and temporal variations in ΔDT also correspond with yield loss change (Fig. 7). Regions with low yield loss probabilities require more intense drought conditions (lower DT values) to induce significant losses. For example, in the Cool/Wet subset of SSP585, SR_E shows lower DT than SR_N and SR_W, with an expanded low ΔDT area projected in the 2080 s. High soil water retention and a favorable climate regime in SR_E may enhance wheat tolerance to water stress (Pinke et al., 2022). In addition to the relatively modest temperature increase and the substantial rise in precipitation, the high plant available water capacity of soils in the SR_E provides a stable water supply for wheat growth under Cool/Wet or Hot/Wet climate scenarios (Fig. S7) (Kukal et al., 2023; Wu et al., 2019). Simultaneously, elevated CO_2 concentrations under such favorable conditions can further enhance photosynthetic efficiency, thereby improving the resilience of crops to drought (Wei et al., 2023), offering a potential explanation for the higher proportion of low drought thresholds anticipated by the 2040 s. Moreover, the extremely high concentrations of CO_2 in the 2080 s under SSP585 may cause the continuous closure of stomata, thus leading to a decrease in photosynthetic efficiency (Hou et al., 2025; Lesk et al., 2021). Therefore, the fertilizer effects of CO_2 may provide adverse damage to the ultimate wheat yield and increase the proportion of high drought thresholds under such conditions.

The uncertainty analysis indicates that the selection of GCMs and copula functions plays a dominant role in the projection results, although the magnitude of influence varies by region (Fig. 8). For wheat yield loss probability and DT, GCMs explain 41.9 % and 41.8 % of the uncertainty in SR_N, 36.5 % and 29.0 % in SR_W, and the contribution drops to approximately 17.2 % and 5.3 % in SR_E, respectively. This regional discrepancy underscores the importance of inter-model

differences in simulating future climatic variables in driving projected drought-related yield loss in more climate-sensitive areas (Bracho-Mujica et al., 2024; Ruane and Mcdermid, 2017). Future climate variability is anticipated to intensify in SR_N, so crop growth is more sensitive to meteorological fluctuations, and even minor variations can result in large deviations in simulation outcomes (Ahmad et al., 2020; Cammarano et al., 2020). In contrast, the SR_W region is projected to experience relatively stable rainfall and temperature patterns under future scenarios, and crops are expected to endure persistent drought stress due to its warm and dry conditions (Li et al., 2024). Accordingly, the uncertainty in risk projections is driven more by the joint distribution of yield and drought index than by regional climatic fluctuations. However, in wetter regions such as SR_E, copula selection becomes increasingly important. Due to the high soil buffer effects (Chen et al., 2020b; Clarke et al., 2021), the relationship between SPAWI and yield in SR_E is weaker than in SR_N and SR_W, even slight soil moisture stress can enhance yield under such conditions (Flohr et al., 2018; Mehraban et al., 2018). Yield losses may not primarily be attributed to agricultural drought in SR_E, thereby increasing sensitivity to the specification of the joint distribution between wheat yield and SPAWI (Xiang et al., 2023).

This study introduces a novel analytical framework that combines a process-based crop model with probabilistic evaluation to assess spatiotemporal patterns of wheat yield loss in response to climate-induced agricultural drought in the NSW wheat belt. The projected increase in drought frequency under climate change scenarios exacerbates the vulnerability of rainfed cropping systems in semi-arid regions (Rahimi-Moghaddam et al., 2023; Wang et al., 2024b). We identified spatial hotspots of increasing drought-related yield risk and quantified the evolving patterns over time. Notably, hotter and drier areas exhibit significantly higher projected risk levels, while wet regions remain relatively stable. The framework can be extended to compound hazards frequently co-occurring in similar climates, such as Mediterranean-type agroecosystems and continental drylands. With minimal recalibration to local soils, cultivar traits, and management calendars, the probabilistic thresholds can be used to map emerging hotspots and to prioritize adaptation portfolios. Additionally, integrating threshold maps with seasonal forecasts and soil-water monitoring would enable early-warning bulletins and stage-targeted advisories. Moreover, these findings suggest that effective drought risk management requires localized adaptation strategies aligned with region-specific climatic and soil conditions. In hot/dry areas, earlier sowing, drought-tolerant cultivars, conservation tillage with residue retention, and fallow management can stabilize yields (Chen et al., 2020a; Li et al., 2024; Wang et al., 2019). In wetter eastern areas, risk remains lower, suggesting a focus on cost-risk optimization and grain-quality safeguards. In addition, given that GCM selection dominates projection spread in arid areas, while copula choices weigh more heavily in wet regions, management strategies should be evaluated under robust-decision frameworks across model subsets.

Some limitations remain in our study. The simulations assumed static soil physical properties under future conditions, without accounting for long-term changes. This assumption implies that interannual changes in soil properties like bulk density are not represented (Liu et al., 2023; Wang and Ren, 2025). This may introduce systematic bias in water balance and crop growth, leading to under- or over-estimation of yield and soil water content. In addition, given that increased drought frequency is often driven by rising temperatures (Gebrechorkos et al., 2025), droughts frequently coincide with heat extremes. Restricting the hazard definition to soil-moisture drought likely underestimates losses where heat and drought co-occur, particularly in hot/dry areas. By capturing exposure but not the full damage pathway under thermal extremes, the approach may yield conservative tail-risk estimates and more lenient drought-trigger thresholds. Part of the projection spread currently attributed to GCM selection or dependence modelling may therefore reflect unmodelled compound events. Integrating these factors into future modelling efforts could yield a more comprehensive understanding of drought-related yield probability and improve projections of crop resilience in semi-arid environments.

5. Conclusion

Our research quantified the spatiotemporal patterns of wheat yield loss probability under agricultural drought in the NSW wheat belt in the context of future climate change. The key findings include:

1. Agricultural drought is projected to intensify in the future, with substantial spatial variability.
2. Low rainfall areas with high temperature show the greatest projected increase in yield loss probability, especially under Hot/Dry subsets.
3. Projected yield loss probability shows greater sensitivity to GCM selection in hot and dry areas, while in warm or wet areas, uncertainty is primarily dominated by the choice of copula functions.

The study highlights the spatial heterogeneity of drought-induced yield losses under climate change, emphasizing the inherent spatial variability in how agricultural drought affects crop production. Regionalized adaptation strategies, tailored drought indicators, and location-specific modelling approaches are thus essential to improve risk assessments and support the resilience of cropping systems in dryland environments.

CRediT authorship contribution statement

Keyu XIANG: Writing – review & editing, Writing – original draft, Validation, Software, Methodology, Data curation, Conceptualization. **Bin Wang:** Writing – review & editing, Validation, Methodology, Conceptualization. **De Li Liu:** Writing – review & editing, Supervision, Software, Methodology, Data curation. **Chao Chen:** Writing – review & editing, Software, Methodology. **Fei Ji:** Writing – review & editing, Methodology. **Shijin Yao:** Validation, Methodology. **Siyi Li:** Software, Data curation. **Alfredo Huete:** Writing – review & editing, Supervision. **Yi Li:** Resources. **Qiang Yu:** Supervision, Resources.

Declaration of Competing Interest

The authors declare that they have no known competing financial interests or personal relationships that could have appeared to influence the work reported in this paper.

Acknowledgement

The first author acknowledges the China Scholarship Council for the financial support of his PhD study (No.202006300006). Facilities for conducting this study were provided by the New South Wales Department of Primary Industries and University of Technology Sydney. Thanks to Grains Research and Development Corporation National Variety Trials, Australia (GRDC-NVT) (https://nvt.grdc.com.au//) for the data support. We are grateful to three anonymous reviewers for their constructive feedback and comments, which have helped to improve the manuscript.

Appendix A. Supporting information

Supplementary data associated with this article can be found in the online version at doi:10.1016/j.eja.2025.127909.

Data availability

Data will be made available on request.

References

Aghakouchak, A., Hao, Z., 2014. A nonparametric multivariate multi-index drought monitoring framework. J. Hydrometeorol. 15, 89–101.

Ahmad, I., Ahmad, B., Boote, K., Hoogenboom, G., 2020. Adaptation strategies for maize production under climate change for semi-arid environments. Eur. J. Agron. 115, 126040.

Ahuja, L.R., Anapalli, S., Feng, G., Feng, P., Flerchinger, G.N., Green, T.R., Hoogenboom, G., Hu, K., Irmak, S., Kersebaum, K.C., Kukal, M.S., Liu, D.L., Lizaso, J.I., Perrier, A., Seyfried, M.S., Shaffer, M.J., Shelia, V., Skaggs, T.H., Stöckle, C.O., Suarez, D.L., Timlin, D.J., Tuzet, A.J., Wang, B., Don Wauchope, R., Wendroth, O., Yu, Q., Modeling Processes and Their Interactions in Cropping Systems Challenges for the 21st Century, John Wiley & Sons, India, 2022.

Bazrafshan, J., Cheraghalizadeh, M., Shahgholian, K., 2022. Development of a non-stationary standardized precipitation evapotranspiration index (NSPEI) for drought monitoring in a changing climate. Water Resour. Manag. 36, 3523–3543.

Bracho-Mujica, G., Rötter, R.P., Haakana, M., Palosuo, T., Fronzek, S., Asseng, S., Yi, C., Ewert, F., Gaiser, T., Kassie, B., Paff, K., Rezaei, E.E., Rodríguez, A., Ruiz-Ramos, M., Srivastava, A.K., Stratonovitch, P., Tao, F., Semenov, M.A., 2024. Effects of changes in climatic means, variability, and agro-technologies on future wheat and maize yields at 10 sites across the globe. Agr. For. Meteor. 346, 109887.

Cammarano, D., Ronga, D., Di Mola, I., Mori, M., Parisi, M., 2020. Impact of climate change on water and nitrogen use efficiencies of processing tomato cultivated in Italy. Agric. Water Manag. 241, 106336.

Cao, Y., Qiu, X., Kang, M., Zhang, L., Lu, W., Liu, B., Tang, L., Xiao, L., Zhu, Y., Cao, W., Liu, L., 2024. Evaluating the impacts of climatic factors and global climate change on the yield and resource use efficiency of winter wheat in China. Eur. J. Agron. 159.

Chen, X., Li, Y., Yao, N., Liu, D.L., Javed, T., Liu, C., Liu, F., 2020b. Impacts of multi-timescale SPEI and SMDI variations on winter wheat yields. Agric. Syst. 185, 102955.

Chen, C., Wang, B., Feng, P., Xing, H., Fletcher, A.L., Lawes, R.A., 2020a. The shifting influence of future water and temperature stress on the optimal flowering period for wheat in Western Australia. Sci. Total Environ. 737, 1–12.

Chen, F., Xu, X., Chen, S., Wang, Z., Wang, B., Zhang, Y., Zhang, C., Feng, P., Hu, K., 2024. Soil buffering capacity enhances maize yield resilience amidst climate perturbations. Agric. Syst. 215, 103870.

Clarke, D., Hess, T.M., Haro-Monteagudo, D., Semenov, M.A., Knox, J.W., 2021. Assessing future drought risks and wheat yield losses in England. Agr. For. Meteor. 297, 108248.

Cui, Y., Jiang, S., Jin, J., Ning, S., Feng, P., 2019. Quantitative assessment of soybean drought loss sensitivity at different growth stages based on S-shaped damage curve. Agric. Water Manag. 213, 821–832.

Dai, P., Nie, J., Yu, Y., Wu, R., 2024. Constraints on regional projections of mean and extreme precipitation under warming. Proc. Natl. Acad. Sci. 121, e2312400121.

Dalgliesh, N., Hochman, Z., Huth, N., Holzworth, D., 2016. Field protocol to APSoil characterisations, 4. CSIRO, Australia, p. 25.

Deihimfard, R., Rahimi-Moghaddam, S., Eyni-Nargeseh, H., Collins, B., 2023. An optimal combination of sowing date and cultivar could mitigate the impact of simultaneous heat and drought on rainfed wheat in arid regions. Eur. J. Agron. 147, 126848.

Dietz, K.J., Zorb, C., Geilfus, C.M., 2021. Drought and crop yield. Plant Biol. (Stuttg.) 23, 881–893.

Dißmann, J., Brechmann, E.C., Czado, C., Kurowicka, D., 2013. Selecting and estimating regular vine copulae and application to financial returns. Comput. Stat. Data Anal. 59, 52–69.

Dubey, N., Ghosh, S., 2023. CO2 fertilization enhances vegetation productivity and reduces ecological drought in India. Environ. Res. Lett. 18, 064025.

Fan, J., Wu, X., Yu, Y., Zuo, Q., Shi, J., Halpern, M., Sheng, J., Jiang, P., Ben-Gal, A., 2023. Characterizing root-water-uptake of wheat under elevated CO2 concentration. Agric. Water Manag. 275, 108005.

Farahmand, A., Aghakouchak, A., 2015. A generalized framework for deriving nonparametric standardized drought indicators. Adv. Water Resour. 76, 140–145.

Feng, P., Liu, D.L., Wang, B., Waters, C., Zhang, M., Yu, Q., 2018a. Projected changes in drought across the wheat belt of southeastern Australia using a downscaled climate ensemble. Int. J. Clim. 39, 1041–1053.

Feng, P., Wang, B., Harrison, M.T., Wang, J., Liu, K., Huang, M., Liu, D.L., Yu, Q., Hu, K., 2022. Soil properties resulting in superior maize yields upon climate warming. Agron. Sust. Dev. 42, 85.

Feng, P., Wang, B., Liu, D.L., Xing, H., Ji, F., Macadam, I., Ruan, H., Yu, Q., 2018b. Impacts of rainfall extremes on wheat yield in semi-arid cropping systems in eastern Australia. Clim. Change 147, 555–569.

Feng, P., Wang, B., Liu, D.L., Waters, C., Yu, Q., 2019. Incorporating machine learning with biophysical model can improve the evaluation of climate extremes impacts on wheat yield in south-eastern Australia. Agr. For. Meteor. 275, 100–113.

Feng, P., Wang, B., Liu, D.L., Waters, C., Xiao, D., Shi, L., Yu, Q., 2020a. Dynamic wheat yield forecasts are improved by a hybrid approach using a biophysical model and machine learning technique. Agr. For. Meteor. 285-286.

Feng, P., Wang, B., Luo, J.J., Liu, L., Waters, C., Ji, F., Ruan, H., Xiao, D., Shi, L., Yu, Q., 2020b. Using large-scale climate drivers to forecast meteorological drought condition in growing season across the Australian wheatbelt. Sci. Total Environ. 724, 138162.

Flohr, B.M., Hunt, J.R., Kirkegaard, J.A., Evans, J.R., Trevaskis, B., Zwart, A., Swan, A., Fletcher, A.L., Rheinheimer, B., 2018. Fast winter wheat phenology can stabilise flowering date and maximise grain yield in semi-arid Mediterranean and temperate environments. Field Crops Res 223, 12–25.

Gajurel, S., Lai, Y., Lobsey, C., Pembleton, K.G., 2024. A cost-effective approach to estimate plant available water capacity. Geoderma 442, 116794.

Gao, S., Huang, S., Singh, V.P., Deng, X., Duan, L., Leng, G., Guo, W., Li, Y., Zhang, L., Han, Z., Huang, Q., 2025. Dynamic response of vegetation to meteorological drought and driving mechanisms in Mongolian Plateau. J. Hydrol. 650, 132541.

Gebrechorkos, S.H., Sheffield, J., Vicente-Serrano, S.M., Funk, C., Miralles, D.G., Peng, J., Dyer, E., Talib, J., Beck, H.E., Singer, M.B., Dadson, S.J., 2025. Warming accelerates global drought severity. Nature 642, 628–635.

Genest, C., Favre, A.-C., 2007. Everything You Always Wanted to Know about Copula Modeling but Were Afraid to Ask. J. Hydrol. Eng. 12, 347–368.

Geng, G., Yang, R., Chen, Q., Deng, T., Yue, M., Zhang, B., Gu, Q., 2023. Tracking the influence of drought events on winter wheat using long-term gross primary production and yield in the Wei River Basin, China. Agric. Water Manag. 275, 1–14.

Godfrey, S.S., Ip, R.H.L., Nordblom, T.L., 2021. Risk Analysis of Australia's Victorian Dairy Farms Using Multivariate Copulae. J. Agric. Appl. Econ. 54, 72–92.

Gringorten, I.I., 1963. A plotting rule for extreme probability paper. J. Geophys. Res. 68, 813–814.

Gu, L., Schumacher, D.L., Fischer, E.M., Slater, L.J., Yin, J., Sippel, S., Chen, J., Liu, P., Knutti, R., 2025. Flash drought impacts on global ecosystems amplified by extreme heat. Nat. Geosci. 1 17.

Gunar, S., Trenkler, D., 1995. Exact and randomization distributions of Kolmogorov-Smirnov tests two or three samples. Comput. Stat. Data Anal. 20, 185–202.

Guo, L., Chen, F., Wang, B., Liu, D.L., Chen, X., Huang, H., Bai, H., Liao, K., Xia, Z., Xiang, K., Li, L., Zheng, T., Yu, Q., 2025a. Developing a multivariate drought index to assess drought characteristics based on the SWAT-Copula method in the Poyang Lake basin, China. Ecol. Indic. 170, 113123.

Guo, W., Huang, S., Liu, L., Leng, G., Huang, Q., Chen, D., Li, P., Wang, Y., Zhu, X., Peng, J., 2025b. Global Critical Drought Thresholds of Terrestrial CarbonSink–Source Transition. Glob. Change Biol. 31, e70129.

Han, Z., Huang, S., Peng, J., Li, J., Leng, G., Huang, Q., Zhao, J., Yang, F., He, P., Meng, X., Li, Z., 2023. GRACE-based dynamic assessment of hydrological drought trigger thresholds induced by meteorological drought and possible driving mechanisms. Remote Sens. Environ. 298, 113831.

Han, Z., Zhang, H., Fu, J., Wang, Z., Duan, L., Zhang, W., Li, Z., 2024. Dynamic assessment of the impact of compound dry-hot conditions on global terrestrial water storage. Remote Sens. Environ. 315, 114428.

Hao, Y., Yuan, X., Zhang, M., 2024. Enhanced relationship between seasonal soil moisture droughts and vegetation under climate change over China. Agr. For. Meteor. 358, 110258.

He, D., Oliver, Y., Rab, A., Fisher, P., Armstrong, R., Kitching, M., Wang, E., 2022. Plant available water capacity (PAWC) of soils predicted from crop yields better reflects within-field soil physicochemical variations. Geoderma 422, 115958.

He, D., Wang, E., 2019. On the relation between soil water holding capacity and dryland crop productivity. Geoderma 353, 11–24.

Holzworth, D.P., Huth, N.I., Devoil, P.G., Zurcher, E.J., Herrmann, N.I., Mclean, G., Chenu, K., Van Oosterom, E.J., Snow, V., Murphy, C., Moore, A.D., Brown, H., Whish, J.P.M., Verrall, S., Fainges, J., Bell, L.W., Peake, A.S., Poulton, P.L., Hochman, Z., Thorburn, P.J., Gaydon, D.S., Dalgliesh, N.P., Rodriguez, D., Cox, H., Chapman, S., Doherty, A., Teixeira, E., Sharp, J., Cichota, R., Vogeler, I., Li, F.Y., Wang, E., Hammer, G.L., Robertson, M.J., Dimes, J.P., Whitbread, A.M., Hunt, J., Van Rees, H., Mcclelland, T., Carberry, P.S., Hargreaves, J.N.G., Macleod, N., Mcdonald, C., Harsdorf, J., Wedgwood, S., Keating, B.A., 2014. APSIM – Evolution towards a new generation of agricultural systems simulation. Environ. Model. Softw. 62, 327–350.

Hosseinzadehtalaei, P., Termonia, P., Tabari, H., 2024. Projected changes in compound hot-dry events depend on the dry indicator considered. Commun. Earth Environ. 5, 220.

Hou, M., Li, Y., Biswas, A., Chen, X., Xie, L., Liu, D., Li, L., Feng, H., Wu, S., Satoh, Y., Pulatov, A., Siddique, K.H.M., 2024. Concurrent drought threatens wheat and maize production and will widen crop yield gaps in the future. Agric. Syst. 220, 104056.

Hou, H., Li, X., Yao, Y., Hu, G., Wang, C., Chu, N., 2025. Attributing future changes in terrestrial evapotranspiration: The combined impacts of climate change, rising CO2, and land use change. Agr. For. Meteor. 373.

Huang, W., Prokhorov, A., 2014. A Goodness-of-fit Test for Copulas. Econom. Rev. 33, 751–771.

Huang, M., Wang, J., Wang, B., Liu, D.L., Feng, P., Yu, Q., Pan, X., Li, S., Jiang, T., 2022. Dominant sources of uncertainty in simulating maize adaptation under future climate scenarios in China. Agric. Syst. 199, 103411.

Hultgren, A., Carleton, T., Delgado, M., Gergel, D.R., Greenstone, M., Houser, T., Hsiang, S., Jina, A., Kopp, R.E., Malevich, S.B., Mccusker, K.E., Mayer, T., Nath, I., Rising, J., Rode, A., Yuan, J., 2025. Impacts of climate change on global agriculture accounting for adaptation. Nature 642, 644–652.

Ipcc, Climate Change 2021: The Physical Science Basis. Contribution of Working Group I to the Sixth Assessment Report of the Intergovernmental Panel on Climate Change., in, Cambridge, United Kingdom and New York, NY, USA, 2021.

Jones, J.W., Antle, J.M., Basso, B., Boote, K.J., Conant, R.T., Foster, I., Godfray, H.C.J., Herrero, M., Howitt, R.E., Janssen, S., Keating, B.A., Munoz-Carpena, R., Porter, C. H., Rosenzweig, C., Wheeler, T.R., 2017. Brief history of agricultural systems modeling. Agric. Syst. 155, 240–254.

Kanthavel, P., Saxena, C.K., Singh, R.K., 2022. Integrated Drought Index based on Vine Copula Modelling. Int. J. Clim. 42, 9510–9529.

Kersebaum, K.C., Stöckle, C.O., 2022. Simulation of climate change effects on evapotranspiration, photosynthesis, crop growth, and yield processes in crop models. Model. Process. Their Interact. Crop. Syst. 291–331.

Kim, Y., Park, H., Kimball, J.S., Colliander, A., Mccabe, M.F., 2023. Global estimates of daily evapotranspiration using SMAP surface and root-zone soil moisture. Remote Sens. Environ. 298, 113803.

Kukal, M.S., Irmak, S., Dobos, R., Gupta, S., 2023. Atmospheric dryness impacts on crop yields are buffered in soils with higher available water capacity. Geoderma 429, 116270.
Lai, X., You, Y., Yang, X., Wang, Z., Shen, Y., 2024. Quantifying the rainfall variability effects on crop growth and production in the intensified annual forage - winter wheat rotation systems in a semiarid region of China. Agric. Water Manag. 305, 109131.
Lesk, C., Coffel, E., Winter, J., Ray, D., Zscheischler, J., Seneviratne, S.I., Horton, R., 2021. Stronger temperature-moisture couplings exacerbate the impact of climate warming on global crop yields. Nat. Food 2, 683–691.
Li, Y., Guan, K., Schnitkey, G.D., Delucia, E., Peng, B., 2019. Excessive rainfall leads to maize yield loss of a comparable magnitude to extreme drought in the United States. Glob. Chang Biol. 25, 2325–2337.
Li, P., Huang, Q., Huang, S., Leng, G., Peng, J., Wang, H., Zheng, X., Li, Y., Fang, W., 2022a. Various maize yield losses and their dynamics triggered by drought thresholds based on Copula-Bayesian conditional probabilities. Agric. Water Manag. 261, 107391.
Li, J., Lei, H., 2022. Impacts of climate change on winter wheat and summer maize dual-cropping system in the North China Plain. Environ. Res. Commun. 4, 075014.
Li, S., Wang, B., Feng, P., Liu, D.L., Li, L., Shi, L., Yu, Q., 2022b. Assessing climate vulnerability of historical wheat yield in south-eastern Australia's wheat belt. Agric. Syst. 196, 103340.
Li, L., Wang, B., Feng, P., Lu, C., Jägermeyr, J., Asseng, S., Luo, J.-J., Harrison, M.T., He, Q., Liu, K., Liu, D.L., Li, Y., Feng, H., Yang, G., Zhao, C., Siddique, K.H.M., Tian, H., Yu, Q., 2025a. Global warming increases the risk of crop yield failures driven by climate oscillations. One Earth, 101318, 101318.
Li, S., Wang, B., Liu, D.L., Chen, C., Feng, P., Huang, M., Wang, X., Shi, L., Waters, C., Huete, A., Yu, Q., 2024. Can agronomic options alleviate the risk of compound drought-heat events during the wheat flowering period in southeastern Australia? Eur. J. Agron. 153, 127030.
Li, S., Wang, B., Liu, D.L., Chen, C., Feng, P., Huete, A., Xiang, K., Yu, Q., 2025b. The contribution of climate drivers to compound drought and extreme temperature events increased in recent decades. Weather Clim. Extrem. 49, 100793.
Li, L., Zhang, Y., Wang, B., Feng, P., He, Q., Shi, Y., Liu, K., Harrison, M.T., Liu, D.L., Yao, N., Li, Y., He, J., Feng, H., Siddique, K.H.M., Yu, Q., 2023. Integrating machine learning and environmental variables to constrain uncertainty in crop yield change projections under climate change. Eur. J. Agron. 149, 126917.
Liu, D.L., Anwar, M.R., O'leary, G., Conyers, M.K., 2014. Managing wheat stubble as an effective approach to sequester soil carbon in a semi-arid environment: spatial modelling. Geoderma 214 (215), 50–61.
Liu, K., Harrison, M.T., Shabala, S., Meinke, H., Ahmed, I., Zhang, Y., Tian, X., Zhou, M., 2020. The state of the art in modeling waterlogging impacts on plants: what do we know and what do we need to know. Earth's. Future 8, 2020EF001801.
Liu, K., Harrison, M.T., Yan, H., Liu, L., Meinke, H., Hoogenboom, G., Wang, B., Peng, B., Guan, K., Jaegermeyr, J., Wang, E., Zhang, F., Yin, X., Archontoulis, S., Nie, L., Badea, A., Man, J., Wallach, D., Zhao, J., Benjumea, A.B., Fahad, S., Tian, X., Wang, W., Tao, F., Zhang, Z., Rotter, R., Yuan, Y., Zhu, M., Dai, P., Nie, J., Yang, Y., Zhang, Y., Zhou, M., 2023. Silver lining to a climate crisis in multiple prospects for alleviating crop waterlogging under future climates. Nat. Commun. 14, 765.
Liu, S., Xiao, L., Sun, J., Yang, P., Yang, X., Wu, W., 2022. Probability of maize yield failure increases with drought occurrence but partially depends on local conditions in China. Eur. J. Agron. 139, 126552.
Liu, D.L., Zuo, H., 2012. Statistical downscaling of daily climate variables for climate change impact assessment over New South Wales, Australia. Clim. Change 115, 629–666.
Ljung, G.M., Box, G.E., 1978. On a measure of lack of fit in time series models. Biometrika 65, 297–303.
Luo, N., Meng, Q., Feng, P., Qu, Z., Yu, Y., Liu, L., Muller, C., Wang, P., 2023. China can be self-sufficient in maize production by 2030 with optimal crop management. Nat. Commun. 14, 2637.
Malik, A., Li, M., Lenzen, M., Fry, J., Liyanapathirana, N., Beyer, K., Boylan, S., Lee, A., Raubenheimer, D., Geschke, A., Prokopenko, M., 2022. Impacts of climate change and extreme weather on food supply chains cascade across sectors and regions in Australia. Nat. Food 3, 631–643.
Mcgrath, J.M., Lobell, D.B., 2013. Regional disparities in the CO2fertilization effect and implications for crop yields. Environ. Res. Lett. 8.
Mehraban, A., Tobe, A., Gholipouri, A., Amiri, E., Ghafari, A., Rostaii, M., 2018. The Effects of Drought Stress on Yield Components, and Yield Stability at Different Growth Stages in Bread Wheat Cultivar (Triticum aestivum L.). Pol. J. Environ. Stud. 28, 739–746.
Messori, G., Muheki, D., Batibeniz, F., Bevacqua, E., Suarez-Gutierrez, L., Thiery, W., 2025. Global mapping of concurrent hazards and impacts associated with climate extremes under climate change. Earth's. Future 13, e2025EF006325.
Nguyen, N.M., Choi, M., 2023. Evapotranspiration partitioning and agricultural drought quantification with an optical trapezoidal framework. Agr. For. Meteor. 338, 109520.
Orlov, A., Jägermeyr, J., Müller, C., Daloz, A.S., Zabel, F., Minoli, S., Liu, W., Lin, T.-S., Jain, A.K., Folberth, C., Okada, M., Poschlod, B., Smerald, A., Schneider, J.M., Sillmann, J., 2024. Human heat stress could offset potential economic benefits of CO2 fertilization in crop production under a high-emissions scenario. One Earth 7, 1250–1265.
Pinke, Z., Decsi, B., Kardos, M.K., Kern, Z., Kozma, Z., Pásztor, L., Ács, T., 2022. Changing patterns of soil water content and relationship with national wheat and maize production in Europe. Eur. J. Agron. 140, 126579.
Qiao, L., Zuo, Z., Zhang, R., Piao, S., Xiao, D., Zhang, K., 2023. Soil moisture-atmosphere coupling accelerates global warming. Nat. Commun. 14, 4908.
Qing, Y., Wang, S., Ancell, B.C., Yang, Z.L., 2022. Accelerating flash droughts induced by the joint influence of soil moisture depletion and atmospheric aridity. Nat. Commun. 13, 1139.
Rahimi-Moghaddam, S., Deihimfard, R., Nazari, M.R., Mohammadi-Ahmadmahmoudi, E., Chenu, K., 2023. Understanding wheat growth and the seasonal climatic characteristics of major drought patterns occurring in cold dryland environments from Iran. Eur. J. Agron. 145, 126772.
Rashid, M.M., Beecham, S., 2019. Development of a non-stationary Standardized Precipitation Index and its application to a South Australian climate. Sci. Total Environ. 657, 882–892.
Rodríguez, P.O., Holzman, M.E., Aldaya, M.M., Rivas, R.E., 2024. Water footprint in rainfed summer and winter crops: the role of soil moisture. Agric. Water Manag. 296, 108787.
Ruane, A.C., Mcdermid, S.P., 2017. Selection of a representative subset of global climate models that captures the profile of regional changes for integrated climate impacts assessment. Earth Perspect. 4, 1–20.
Ruane, A.C., Phillips, M., Jägermeyr, J., Müller, C., 2024. Non-linear climate change impacts on crop yields may mislead stakeholders. Earth's. Future 12, e2023EF003842.
Sakamoto, Y., Ishiguro, M., Kitagawa, G., 1986. Akaike information criterion statistics. Dordrecht, The Netherlands. D. Reidel 81, 26853.
Schaeffer, R., Schipper, E.L.F., Ospina, D., Mirazo, P., Alencar, A., Anvari, M., Artaxo, P., Biresselioglu, M.E., Blome, T., Boeckmann, M., Brink, E., Broadgate, W., Bustamante, M., Cai, W., Canadell, J.G., Cardinale, R., Chidichimo, M.P., Ditlevsen, P., Eicker, U., Feron, S., Fikru, M.G., Fuss, S., Gaye, A.T., Gustafsson, Ö., Harring, N., He, C., Hebden, S., Heilemann, A., Hirota, M., Janardhanan, N., Juhola, S., Jung, T.Y., Kejun, J., Kilkiş, Ş., Kumarasinghe, N., Lapola, D., Lee, J.-Y., Levis, C., Lusambili, A., Maasakkers, J.D., Macintosh, C., Mahmood, J., Mankin, J.S., Marchegiani, P., Martin, M., Mukherji, A., Muñoz-Erickson, T.A., Niazi, Z., Nyangon, J., Pandipati, S., Perera, A.T.D., Persad, G., Persson, Å., Redman, A., Riipinen, I., Rockström, J., Roffe, S., Roy, J., Sakschewski, B., Samset, B.H., Schlosser, P., Sharifi, A., Shih, W.-Y., Sioen, G.B., Sokona, Y., Stammer, D., Suk, S., Thiam, D., Thompson, V., Tullos, E., Van Westen, R.M., Vargas Falla, A.M., Vecellio, D.J., Worden, J., Wu, H.C., Xu, C., Yang, Y., Zachariah, M., Zhang, Z., Ziervogel, G., 2025. Ten new insights in climate science 2024. One Earth 8, 101285.
Seo, J., Won, J., Lee, H., Kim, S., 2024. Probabilistic monitoring of meteorological drought impacts on water quality of major rivers in South Korea using copula models. Water Res. 251, 121175.
Shi, L., Feng, P., Wang, B., Liu, D.L., Zhang, H., Liu, J., Yu, Q., 2022. Assessing future runoff changes with different potential evapotranspiration inputs based on multi-model ensemble of CMIP5 projections. J. Hydrol. 612, 128042.
Sklar, A., 1973. Random variables, joint distribution functions, and copulas. Kybernetika 9, 449–460.
Slater, L.J., Huntingford, C., Pywell, R.F., Redhead, J.W., Kendon, E.J., 2022. Resilience of UK crop yields to compound climate change. Earth Syst. Dyn. 13, 1377–1396.
Smith, M.D., Wilkins, K.D., Holdrege, M.C., Wilfahrt, P., Collins, S.L., Knapp, A.K., Sala, O.E., Dukes, J.S., Phillips, R.P., Yahdjian, L., Gherardi, L.A., Ohlert, T., Beier, C., Fraser, L.H., Jentsch, A., Loik, M.E., Maestre, F.T., Power, S.A., Yu, Q., Felton, A.J., Munson, S.M., Luo, Y., Abdoli, H., Abedi, M., Alados, C.L., Alberti, J., Alon, M., An, H., Anacker, B., Anderson, M., Auge, H., Bachle, S., Bahalkeh, K., Bahn, M., Batbaatar, A., Bauerle, T., Beard, K.H., Behn, K., Beil, I., Biancari, L., Blindow, I., Bondaruk, V.F., Borer, E.T., Bork, E.W., Bruschetti, C.M., Byrne, K.M., Cahill Jr., J.F., Calvo, D.A., Carbognani, M., Cardoni, A., Carlyle, C.N., Castillo-Garcia, M., Chang, S.X., Chieppa, J., Cianciaruso, M.V., Cohen, O., Cordeiro, A.L., Cusack, D.F., Dahlke, S., Daleo, P., D'antonio, C.M., Dietterich, L.H., T., S.D., Dubbert, M., Ebeling, A., Eisenhauer, N., Fischer, F.M., Forte, T.G.W., Gebauer, T., Gozalo, B., Greenville, A.C., Guidoni-Martins, K.G., Hannusch, H.J., Vatso Haugum, S., Hautier, Y., Hefting, M., Henry, Ha.L., Hoss, D., Ingrisch, J., Iribarne, O., Isbell, F., Johnson, Y., Jordan, S., Kelly, E.F., Kimmel, K., Kreyling, J., Kroel-Dulay, G., Kropfl, A., Kubert, A., Kulmatiski, A., Lamb, E.G., Larsen, K.S., Larson, J., Lawson, J., Leder, C.V., Linstadter, A., Liu, J., Liu, S., Lodge, A.G., Longo, G., Loydi, A., Luan, J., Curtis Lubbe, F., Macfarlane, C., Mackie-Haas, K., Malyshev, A.V., Maturano-Ruiz, A., Merchant, T., Metcalfe, D.B., Mori, A.S., Mudongo, E., Newman, G.S., Nielsen, U.N., Nimmo, D., Niu, Y., Nobre, P., O'connor, R.C., Ogaya, R., Onatibia, G.R., Orban, I., Osborne, B., Otfinowski, R., Partel, M., Penuelas, J., Peri, P.L., Peter, G., Petraglia, A., Picon-Cochard, C., Pillar, V.D., Pineiro-Guerra, J.M., Ploughe, L.W., Plowes, R.M., Portales-Reyes, C., Prober, S.M., Pueyo, Y., Reed, S.C., Ritchie, E.G., Rodriguez, D.A., Rogers, W.E., Roscher, C., Sanchez, A.M., Santos, B.A., Cecilia Scarfo, M., Seabloom, E.W., Shi, B., Souza, L., Stampfli, A., Standish, R.J., Sternberg, M., Sun, W., Sunnemann, M., Tedder, M., Thorvaldsen, P., Tian, D., Tielborger, K., Valdecantos, A., Van Den Brink, L., Vandvik, V., Vankoughnett, M.R., Guri Velle, L., Wang, C., Wang, Y., Wardle, G.M., Werner, C., Wei, C., Wiehl, G., Williams, J.L., Wolf, A.A., Zeiter, M., Zhang, F., Zhu, J., Zong, N., Zuo, X., 2024. Extreme drought impacts have been underestimated in grasslands and shrublands globally. Proc. Natl. Acad. Sci., e2309881120
Sun, J., Sun, S., Yin, Y., Wang, Y., Zhao, J., Tang, Y., Wu, P., 2024. Decoupling trend and drivers between grain water-carbon footprint and economy-ecology development in China. Agric. Syst. 217, 103904.
Tang, J., Niu, B., Hu, Z., Zhang, X., 2024. Increasing susceptibility and shortening response time of vegetation productivity to drought from 2001 to 2021. Agr. For. Meteor. 352, 110025.
Tausz-Posch, S., Tausz, M., Bourgault, M., 2020. Elevated [CO(2(2)effects on crops: advances in understanding acclimation, nitrogen dynamics and interactions with drought and other organisms. Plant Biol. (Stuttg.) 22 (1), 38–51.

Tefera, M.L., Seddaiu, G., Carletti, A., Awada, H., 2024. Rainfall variability and drought in West Africa: challenges and implications for rainfed agriculture. Theor. Appl. Climatol. 156, 1–21.
Tepegjozova, M., Zhou, J., Claeskens, G., Czado, C., 2022. Nonparametric C- and D-vine-based quantile regression. Depend. Model. 10, 1–21.
Toreti, A., Deryng, D., Tubiello, F.N., Muller, C., Kimball, B.A., Moser, G., Boote, K., Asseng, S., Pugh, Ta.M., Vanuytrecht, E., Pleijel, H., Webber, H., Durand, J.L., Dentener, F., Ceglar, A., Wang, X., Badeck, F., Lecerf, R., Wall, G.W., Van Den Berg, M., Hoegy, P., Lopez-Lozano, R., Zampieri, M., Galmarini, S., O'leary, G.J., Manderscheid, R., Mencos Contreras, E., Rosenzweig, C., 2020. Narrowing uncertainties in the effects of elevated CO(2(2)n crops. Nat. Food 1, 775–782.
Ukkola, A.M., De Kauwe, M.G., Roderick, M.L., Abramowitz, G., Pitman, A.J., 2020. Robust future changes in meteorological drought in CMIP6 projections despite uncertainty in precipitation. Geophys. Res. Lett. 47, 2020GL087820.
Vicente-Serrano, S.M., Beguería, S., López-Moreno, J.I., 2010. A multiscalar drought index sensitive to global warming: the standardized precipitation evapotranspiration index. J. Clim. 23, 1696–1718.
Wang, B., Feng, P., Chen, C., Liu, D.L., Waters, C., Yu, Q., 2019. Designing wheat ideotypes to cope with future changing climate in South-Eastern Australia. Agric. Syst. 170, 9–18.
Wang, B., Jägermeyr, J., O'leary, G.J., Wallach, D., Ruane, A.C., Feng, P., Li, L., Liu, D.L., Waters, C., Yu, Q., Asseng, S., Rosenzweig, C., 2024a. Pathways to identify and reduce uncertainties in agricultural climate impact assessments. Nature Food.
Wang, B., Li, L., Feng, P., Chen, C., Luo, J.-J., Taschetto, A.S., Harrison, M.T., Liu, K., Liu, D.L., Yu, Q., Guo, X., 2024b. Probabilistic analysis of drought impact on wheat yield and climate change implications. Weather Clim. Extrem. 45, 100708.
Wang, B., Liu, D.L., Asseng, S., Macadam, I., Yu, Q., 2015. Impact of climate change on wheat flowering time in eastern Australia. Agr. For. Meteor. 209-210, 11–21.
Wang, B., Liu, D.L., Asseng, S., Macadam, I., Yu, Q., 2017. Modelling wheat yield change under CO2 increase, heat and water stress in relation to plant available water capacity in eastern Australia. Eur. J. Agron. 90, 152–161.
Wang, L., Ren, W., 2025. Drought in agriculture and climate-smart mitigation strategies. Cell Rep. Sustain. 2, 100386.
Wang, Z., Wang, C., 2023. Interactive effects of elevated temperature and drought on plant carbon metabolism: a meta-analysis. Glob. Chang Biol. 29, 2824–2835.
Wei, Q., Pan, H., Yang, Y., Tan, S., Zheng, L., Wang, H., Zhang, J., Zhang, Z., Wei, Y., Wang, X., Ma, X., Xiong, S., 2023. Effects of elevated atmospheric [CO(2(2)on grain starch characteristics in different specialized wheat. Front. Plant Sci. 14, 1334053.
White, H., 1982. Maximum likelihood estimation of misspecified models. Économ. J. Econom. Soc. 1982 1–25.
Workneh, H.T., Chen, X., Ma, Y., Bayable, E., Dash, A., 2024. Comparison of IDW, Kriging and orographic based linear interpolations of rainfall in six rainfall regimes of Ethiopia. J. Hydrol. Reg. Stud. 52, 101696.
Wu, R., Lawes, R., Oliver, Y., Fletcher, A., Chen, C., 2019. How well do we need to estimate plant-available water capacity to simulate water-limited yield potential? Agric. Water Manag. 212, 441–447.
Wu, H., Su, X., Huang, S., Singh, V.P., Zhou, S., Tan, X., Hu, X., 2025. Decreasing dynamic predictability of global agricultural drought with warming climate. Nat. Clim. Change 15 411419.
Xiang, K., Wang, B., Liu, D.L., Chen, C., Waters, C., Huete, A., Yu, Q., 2023. Probabilistic assessment of drought impacts on wheat yield in south-eastern Australia. Agric. Water Manag. 284, 108359.
Xiang, K., Wang, B., Liu, D.L., Chen, C., Ji, F., Yang, Y., Li, S., Huang, M., Huete, A., Yu, Q., 2025. Soil with high plant available water capacity can mitigate the risk of wheat growth under drought conditions in southeastern Australia. Eur. J. Agron. 164, 127460.
Xiang, K., Zhang, X., Peng, X., Yao, N., Biswas, A., Liu, D., Zou, Y., Pulatov, B., Li, Y., Liu, F., 2022. Differences in spatiotemporal variability of potential and reference crop evapotranspirations. Water 14.
Xie, L., Li, Y., Zhang, Z., Siddique, K.H.M., Song, X., 2025. Exploring the combined effects of drought and drought-flood abrupt alternation on vegetation using interpretable machine learning model and r-vine copula function. Agr. For. Meteor. 370, 110568.
Yang, C., Liu, C., Gu, Y., Wang, Y., Xing, X., Ma, X., 2023. A novel comprehensive agricultural drought index accounting for precipitation, evapotranspiration, and soil moisture. Ecol. Indic. 154, 110593.
Yang, C., Liu, C., Liu, Y., Gao, Y., Xing, X., Ma, X., 2024. Prediction of drought trigger thresholds for future winter wheat yield losses in China based on the DSSAT-CERES-Wheat model and Copula conditional probabilities. Agric. Water Manag. 299, 108881.
Yao, S., Wang, B., Liu, D.L., Li, S., Ruan, H., Yu, Q., 2025. Assessing the impact of climate variability on Australia's sugarcane yield in 1980–2022. Eur. J. Agron. 164.
Ye, Z., Qiu, X., Chen, J., Cammarano, D., Ge, Z., Ruane, A.C., Liu, L., Tang, L., Cao, W., Liu, B., Zhu, Y., 2020. Impacts of 1.5 °C and 2.0 °C global warming above pre-industrial on potential winter wheat production of China. Eur. J. Agron. 120, 126149.
Yerdelen, C., Abdelkader, M., Eris, E., 2021. Assessment of drought in SPI series using continuous wavelet analysis for Gediz Basin, Turkey. Atmo. Res. 260, 105687.
Zhang, Y., Li, C., Chiew, F.H.S., Post, D.A., Zhang, X., Ma, N., Tian, J., Kong, D., Leung, L. R., Yu, Q., Shi, J., Liu, C., 2023a. Southern Hemisphere dominates recent decline inglobal water availability. Science 382, 579–584.
Zhang, Y., Liu, X., Jiao, W., Wu, X., Zeng, X., Zhao, L., Wang, L., Guo, J., Xing, X., Hong, Y., 2023b. Spatial heterogeneity of vegetation resilience changes to different drought types. Earth's. Future 11, 2022EF003108.
Zhang, C., Wang, Y., Jia, X., Shao, M.A., An, Z., 2020. Variations in capacity and storage of plant-available water in deep profiles along a revegetation and precipitation gradient. J. Hydrol. 581.
Zhang, L., Yuan, F., He, X., 2024. Probabilistic assessment of global drought recovery and its response to precipitation changes. Geophys. Res. Lett. 51, 2023GL106067.
Zhao, M., A, G., Liu, Y., Konings, A.G., 2022. Evapotranspiration frequently increases during droughts. Nat. Clim. Change 12, 1024–1030.
Zhao, J., Peng, H., Yang, J., Huang, R., Huo, Z., Ma, Y., 2024. Response of winter wheat to different drought levels based on Google Earth Engine in the Huang-Huai-Hai Region, China. Agric. Water Manag. 292, 108662.
Zheng, B., Chenu, K., Doherty, A., Chapman, S., 2015. The APSIM-Wheat Module.
Zhou, Z., Wang, P., Li, L., Fu, Q., Ding, Y., Chen, P., Xue, P., Wang, T., Shi, H., 2024. Recent development on drought propagation A comprehensive review. J. Hydrol. 645, 132196.